An Active Perception Framework for Autonomous Underwater Vehicle Navigation Under Sensor Constraints

Dongsik Chang, *Member, IEEE*, Matthew Johnson-Roberson, and Jing Sun, *Fellow, IEEE*

***Abstract*— Inertial navigation for autonomous underwater vehicles (AUVs) is challenging because of the drift error caused by the noise and measurement errors of inertial sensors, typically packaged as an inertial measurement unit (IMU), integrated over time. To mitigate the drift error, recent AUV state estimation approaches incorporate external references or environmental information obtained from exteroceptive sensors, with increased costs and limited operational domains. For improved navigation under sensor constraints, this article proposes an active perception framework that exploits vehicle motion to estimate the flow state together with the vehicle state using IMU and depth sensors only. The proposed framework uses the estimated flow state as external information to improve vehicle state estimation. We construct a linear time-varying system for the flow state, separated from a nonlinear system for the vehicle state. This formulation allows us to analyze uniform complete observability for the flow state, which is found to depend on vehicle motion. Then, along with vehicle and flow state estimators, we design a vehicle controller to enable vehicle motion to maximize an information metric pertaining to estimation performance based on either observability or constructability Gramian for the flow state. The proposed framework is validated through simulations for a case study with a vehicle descending through the water column in a time-varying flow field. The effectiveness of the framework is demonstrated by comparing results obtained from its four implementations with those from baseline approaches without active perception.**

***Index Terms*— Active perception, inertial navigation, mid-water localization, underwater localization, underwater navigation.**

I. Introduction

AUTONOMOUS underwater vehicles (AUVs) have significantly advanced in their capability of collecting data for environmental monitoring and exploration in coastal areas and deep oceans [1]. However, since the global positioning system (GPS) is not available underwater, AUV navigation has been challenging. A conventional approach for underwater navigation is inertial navigation based on dead reckoning using inertial sensors, typically packaged as an inertial measurement unit (IMU), that is, the position and orientation of the vehicle are calculated by integrating linear acceleration and angular velocity measurements from an IMU. However, due to the sensor noise and measurement errors integrated over time, inertial navigation suffers from the position error that grows over the course of the mission unless the error, also known as the drift error, is corrected using external references, e.g., through GPS updates.

Since regular surfacing of a vehicle for GPS updates is not desirable for many underwater missions, other approaches have been proposed to mitigate the drift error using information obtained from exteroceptive sensors as references [2]–[4]. For example, acoustic positioning systems can provide vehicle position information relative to beacons, but they require either the presence of a dedicated surface vessel during the mission or the deployment of transponders prior to the mission. Optical and acoustic sensors, such as cameras and sonar sensors, are used to capture environmental information, such as features of static landmarks to calculate the vehicle position relative to the landmarks. Doppler velocity logs (DVLs) measure vehicle velocity relative to the sea bottom, which is used to estimate vehicle position. However, these sensors are typically expensive and provide effective information only when the vehicle stays close to the landmarks or the sea bottom.

In addition to positional reference information, another information available from exteroceptive sensors is the velocity of ocean flow (e.g., ocean currents) around a vehicle. Since ocean flow introduces perturbations to vehicle operations [5]–[7], flow velocity estimation combined with vehicle pose estimation has been studied to improve vehicle navigation. For example, flow estimation has been studied by using vehicle position information obtained from acoustic positioning systems (e.g., [8], [9]) and also by using measurements of surrounding water velocity relative to the vehicle obtained from acoustic Doppler current profilers (ADCPs) (e.g., [10]–[14]). The latter approaches with ADCPs may work effectively in unstructured regions without limiting the operational domain of a vehicle, but they incur significant costs.

With further analysis on the coupling between vehicle motion and ocean flow, our previous work [15] has found that this coupling provides a mechanism to obtain information about ocean flow from vehicle motion, in which by leveraging

Manuscript received July 25, 2021; accepted December 17, 2021. Manuscript received in final form December 27, 2021. Recommended by Associate Editor W. He. *(Corresponding author: Dongsik Chang.)*

Dongsik Chang was with the Department of Naval Architecture and Marine Engineering, University of Michigan, Ann Arbor, MI 48109 USA. He is now with the Collaborative Robotics and Intelligent Systems Institute, Oregon State University, Corvallis, OR 97331 USA (e-mail: changdo@oregonstate.edu).

Matthew Johnson-Roberson and Jing Sun are with the Department of Naval Architecture and Marine Engineering, University of Michigan, Ann Arbor, MI 48109 USA (e-mail: mattjr@umich.edu; jingsun@umich.edu).

Color versions of one or more figures in this article are available at https://doi.org/10.1109/TCST.2021.3139307.

Digital Object Identifier 10.1109/TCST.2021.3139307

spiral motion of a vehicle (e.g., [16]–[18]) which generates a three-dimensional (3-D) helical trajectory through the water column, flow velocity is estimated from the IMU measurement through *active perception* (e.g., [19], [20]). Then, this flow estimate is used to improve vehicle localization using IMU and depth sensors only. This finding is consistent with the analysis in [16], which shows that the spiral motion with an acoustic positioning system can ensure observability, and [10], which demonstrates that increased complexity of vehicle motion with DVL and depth sensor measurements helps to reduce the unobservable subspace. However, the aforementioned studies employ exteroceptive sensors, and neither take the coupling between vehicle motion and ocean flow into account nor incorporate ocean flow estimation in vehicle navigation.

Extending our previous work [15], this article proposes an active perception framework for underwater navigation that exploits vehicle motion to estimate the flow state together with the vehicle state without requiring spiral motion and exteroceptive sensors. The study in this article assumes sensor constraints in the sense that only IMU and depth sensors are used. To facilitate flow state estimation, we construct a linear time-varying system for the flow state, separated from a nonlinear system for the vehicle state. While the vehicle and flow states are estimated by separate estimators, the coupling between vehicle motion and ocean flow is explored in the design of the estimators. In addition, this coupling causes the observability for the flow state to depend on vehicle motion, thereby providing an opportunity for active perception to enhance flow state estimation. Active perception in this article specifically refers to improving flow state estimation through active vehicle motion control.

For the perception part of active perception, we consider the following two information metrics for the flow state: 1) observability Gramian and 2) constructability Gramian. These two metrics are connected in terms of uniform complete observability, which is a property related to the convergence of state estimation. For the action part, we design a vehicle controller to minimize the maximum variance of flow state estimation based on either observability or constructability Gramian. Then, the estimated flow is incorporated in vehicle state estimation to improve navigation performance. The proposed framework is validated through simulations for a case study in which a vehicle, modeled as our testbed AUV with a commercial-grade IMU, descends through the water column in a time-varying flow field. In this case study, the control objective is to improve flow estimation without goal and depth constraints. By using simulated IMU and depth sensor measurements, the proposed framework simultaneously estimates the vehicle and flow states, while two baseline approaches without active perception estimate the vehicle state only. The effectiveness of the active perception framework is demonstrated by comparing results obtained from its four implementations with those from the baseline approaches.

Active perception for AUVs has been leveraged for various applications, including information gathering [21], simultaneous localization and mapping [22], target tracking [23], and plume source localization [24]. Previous work on active perception has focused on improving navigation by maximizing information collected from exteroceptive sensors. To the best of our knowledge, this is the first work on underwater navigation that incorporates active perception to design vehicle control for improved flow estimation and subsequently enhanced navigation without using exteroceptive sensors, such as ADCP/DVLs and acoustic positioning systems. While the proposed framework is demonstrated for a simple case study, please note that the framework can be extended to various navigation tasks where the dependence of flow state observability on vehicle motion can be identified and exploited in control design.

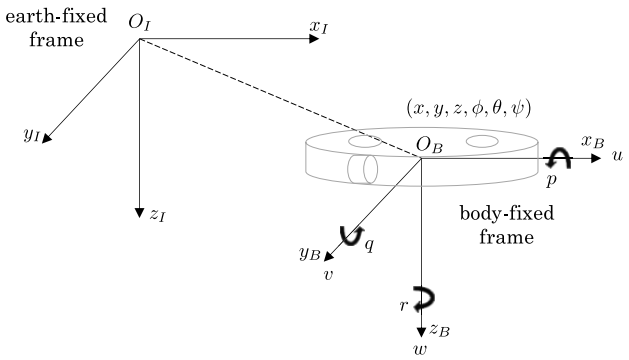

Fig. 1. Body- and Earth-fixed frames for the vehicle motion model.

The rest of this article is organized as follows. Section II introduces the preliminaries for the research work presented in this article and Section III details the active perception problem. Next, Section IV presents systems for vehicle and flow state estimation and analyzes observability for the flow state in relation to vehicle motion. Then, Section V presents our proposed active perception framework for underwater navigation, and Section VI discusses simulation results. Finally, Section VII concludes this article.

II. Preliminaries

This section presents preliminaries for our study. First, a general vehicle motion model in the presence of ocean flow is introduced. Then, a short description of our testbed AUV, which motivated our study, is provided.

A. General Vehicle Motion Model

For our analysis on the coupling between vehicle motion and ocean flow, we use a six-degree-of-freedom (DOF) vehicle motion model. The pose and velocity of the vehicle are described using two coordinate frames: Earth-fixed, which is also often referred to as inertial, and body-fixed (see Fig. 1). The origin of the Earth-fixed frame, O_I, is often fixed at a reference position at the surface of water, e.g., the position of a mother ship. The origin of the body-fixed frame, O_B, is the reference position of the vehicle and often conveniently chosen as the center of mass of the vehicle.

Let us denote the position and orientation of the vehicle in the Earth-fixed frame by $\boldsymbol{\eta}_1 = [x, y, z]^T \in \mathbb{R}^3$ and $\boldsymbol{\eta}_2 = [\phi, \theta, \psi]^T \in \mathbb{R}^3$, respectively. Together, the pose of the vehicle is defined by $\boldsymbol{\eta} = [\boldsymbol{\eta}_1^T, \boldsymbol{\eta}_2^T]^T \in \mathbb{R}^6$. With the linear and angular

velocities of the vehicle in the body-fixed frame denoted by $\boldsymbol{\nu}_1 = [u, v, w]^T \in \mathbb{R}^3$ and $\boldsymbol{\nu}_2 = [p, q, r]^T \in \mathbb{R}^3$, respectively, the velocity of the vehicle is represented by $\boldsymbol{\nu} = [\boldsymbol{\nu}_1^T, \boldsymbol{\nu}_2^T]^T \in \mathbb{R}^6$. For coordinate transformation from the body-fixed frame to the Earth-fixed frame, we define

$$J(\boldsymbol{\eta}_2) = \begin{bmatrix} {}^I_B R(\boldsymbol{\eta}_2) & 0_{3\times3} \\ 0_{3\times3} & T_\Theta(\boldsymbol{\eta}_2) \end{bmatrix} \in \mathbb{R}^{6\times6} \tag{1}$$

where ${}^I_B R(\boldsymbol{\eta}_2) \in \mathbb{R}^{3\times3}$ and $T_\Theta(\boldsymbol{\eta}_2) \in \mathbb{R}^{3\times3}$ transform linear velocity and angular velocity, respectively (see [25], [26] for details).

While underwater, the motion of the vehicle is affected by ocean flow. Let us define flow velocity that affects vehicle motion, expressed in the body-fixed frame, by $\mathbf{f} = [f_u, f_v, f_w, f_p, f_q, f_r]^T \in \mathbb{R}^6$ with its linear and angular components defined as $\mathbf{f}_1 = [f_u, f_v, f_w]^T \in \mathbb{R}^3$ and $\mathbf{f}_2 = [f_p, f_q, f_r]^T \in \mathbb{R}^3$, respectively. The corresponding flow velocity in the Earth-fixed frame, denoted by $\mathbf{f}^I = [f_x, f_y, f_z, f_\phi, f_\theta, f_\psi]^T \in \mathbb{R}^6$, is obtained by $\mathbf{f}^I = J(\boldsymbol{\eta}_2)\mathbf{f}$. The linear and angular components of $\mathbf{f}^I$ are defined by $\mathbf{f}_1^I = [f_x, f_y, f_z]^T \in \mathbb{R}^3$ and $\mathbf{f}_2^I = [f_\phi, f_\theta, f_\psi]^T \in \mathbb{R}^3$, respectively.

With the notations defined above, the motion of the AUV can be generally described by

$$\dot{\boldsymbol{\eta}} = J(\boldsymbol{\eta}_2)\boldsymbol{\nu} \tag{2}$$

$$M_{\mathrm{RB}}\dot{\boldsymbol{\nu}} + M_A\dot{\boldsymbol{\nu}}_r + C_{\mathrm{RB}}(\boldsymbol{\nu})\boldsymbol{\nu} + C_A(\boldsymbol{\nu}_r)\boldsymbol{\nu}_r + D(\boldsymbol{\nu}_r)\boldsymbol{\nu}_r\boldsymbol{\sigma}(\boldsymbol{\eta}) = \boldsymbol{\tau} \tag{3}$$

where $\boldsymbol{\nu}_r = \boldsymbol{\nu} - \mathbf{f}$ is the vehicle velocity relative to flow (see [25] for details). Equations (2) and (3) represent vehicle kinematics and dynamics, respectively. Terms $M_{\mathrm{RB}} \in \mathbb{R}^{6\times6}$ and $M_A \in \mathbb{R}^{6\times6}$ are the rigid body and added mass matrices, respectively, $C_{\mathrm{RB}} \in \mathbb{R}^{6\times6}$ and $C_A \in \mathbb{R}^{6\times6}$ are the Coriolis and centripetal matrices induced by the rigid body and added mass, respectively, $D \in \mathbb{R}^{6\times6}$ is the hydrodynamic damping matrix, $\boldsymbol{\sigma} \in \mathbb{R}^6$ is the vector of restoring forces and moments, and $\boldsymbol{\tau} = [\tau_u, \tau_v, \tau_w, \tau_p, \tau_q, \tau_r]^T \in \mathbb{R}^6$ is the vector of input forces and moments.

For simplicity, we only consider the diagonal terms in M_A and quadratic diagonal terms in D such that

$$M_A = -\mathrm{diag}(X_{\dot{u}}, Y_{\dot{v}}, Z_{\dot{w}}, K_{\dot{p}}, M_{\dot{q}}, N_{\dot{r}}) \tag{4}$$

$$D = -\mathrm{diag}(X_{|u|u}, Y_{|v|v}, Z_{|w|w}, K_{|p|p}, M_{|q|q}, N_{|r|r}) \cdot |\boldsymbol{\nu}_r| \tag{5}$$

where diag represents a matrix formed with the elements being its diagonal entries. Terms $X_{\dot{u}}$, $Y_{\dot{v}}$, $Z_{\dot{w}}$, $K_{\dot{p}}$, $M_{\dot{q}}$, and $N_{\dot{r}}$ are the linear added mass coefficients, and $X_{|u|u}$, $Y_{|v|v}$, $Z_{|w|w}$, $K_{|p|p}$, $M_{|q|q}$, and $N_{|r|r}$ are the quadratic damping coefficients.

As can be seen from (2) and (3), vehicle motion and ocean flow are tightly coupled. Their interplay serves as the analytic foundation for the formulation of the proposed active perception framework, which is shown in Fig. 2.

B. Testbed AUV: DROP-Sphere

This study is motivated by deep-sea research being conducted in the Deep Robot Optical Perception (DROP) Laboratory, University of Michigan. Our testbed AUV, *DROP-Sphere*

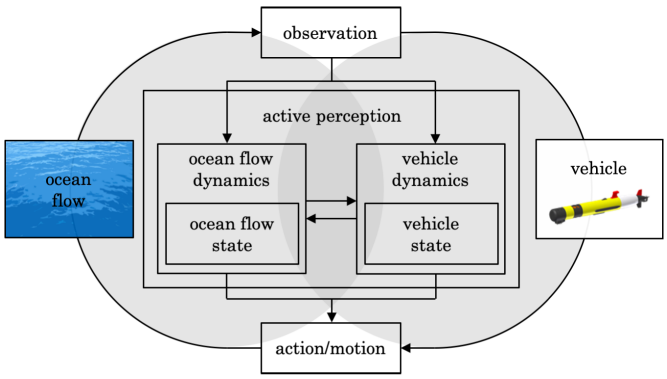

Fig. 2. Block diagram of the concept of active perception in our approach.

Fig. 3. Image of DROP-Sphere.

(see Fig. 3), developed by the DROP Laboratory, is open-source, low-cost, and rated for 6000-m operational depth for optical benthic mapping in the deep sea. The major electronic and computing devices (e.g., battery, camera, and microprocessor) are mounted inside a transparent sphere located at the center of the vehicle. The vehicle carries an IMU (Xsens MTi-30) and a depth sensor (TE MS5837) as its primary navigational sensors. The vehicle has two pairs of thrusters for horizontal and vertical motions. With the four thrusters, control input $\boldsymbol{\tau}$ in (3) is given by $\boldsymbol{\tau} = B \times [T_1, T_2, T_3, T_4]^T$ where

$$B = \begin{bmatrix} 0 & 0 & 1 & 1 \\ 0 & 0 & 0 & 0 \\ 1 & 1 & 0 & 0 \\ 0 & 0 & 0 & 0 \\ 0.279 & -0.279 & 0 & 0 \\ 0 & 0 & 0.169 & -0.169 \end{bmatrix} \in \mathbb{R}^{6\times4} \tag{6}$$

is a thrust allocation matrix and $T_i \in \mathbb{R}, i \in \{1, 2, 3, 4\}$ is thrust input with $\{1, 2\}$ for vertical thrust and $\{3, 4\}$ for horizontal thrust.

Tables I and II show the specifications and model parameters of DROP-Sphere, respectively. The dimension of the vehicle is 0.86 m long, 0.43 m width, and 0.25 m height, and its mass and displacement are 20.42 and 20.57 kg, respectively. Note that the vehicle is positive buoyant with its weight and buoyancy approximated as 200.3202 and 201.7917 N for gravity $g = 9.81$ m/s^2 in this article, respectively. Its centers of buoyancy and gravity are $\mathbf{r}_B = [0.0, 0.0, 0.0]^T$ and $\mathbf{r}_G^{\mathrm{true}} = [0.00295, 0.00054, 0.00219]^T$ m, respectively. The water density ρ is set to 1025 kg/m^3 in this article. For benthic mapping, we make this positive buoyant vehicle temporarily negative buoyant by attaching a drop weight at $\mathbf{r}_w = [0.431, 0.0, 0.0]^T$ m so that the vehicle can descend through the water column without using its active propulsion

TABLE I
SPECIFICATIONS OF DROP-SPHERE

Item	Value [Unit]	Item	Value [Unit]
Length	0.86 $[m]$	Width	0.43 $[m]$
Height	0.25 $[m]$	Max depth	6000 $[m]$
Mass	20.42 $[kg]$	Displacement	20.57 $[kg]$
Power	210 $[Wh]$	Cost	< 30000 [USD]

TABLE II
MODEL PARAMETERS OF DROP-SPHERE

Parameter	Value [Unit]	Parameter	Value [Unit]
I_{xx}	0.1205 $[kg \cdot m^2]$	I_{yy}	0.9431 $[kg \cdot m^2]$
I_{zz}	1.0061 $[kg \cdot m^2]$	$X_{\dot{u}}$	-2.042 $[kg]$
$Y_{\dot{v}}$	-32.2013 $[kg]$	$Z_{\dot{w}}$	-32.2013 $[kg]$
$K_{\dot{p}}$	-0.0805 $[kg]$	$M_{\dot{q}}$	-2.6834 $[kg]$
$N_{\dot{r}}$	-2.6834 $[kg]$	$X_{\|u\|u}$	-48.17 $[kg/m]$
$Y_{\|v\|v}$	-4.11 $[kg/m]$	$Z_{\|w\|w}$	-4.11 $[kg/m]$
$K_{\|p\|p}$	-48.17 $[kg/m]$	$M_{\|q\|q}$	-4.11 $[kg/m]$
$N_{\|r\|r}$	-4.11 $[kg/m]$	ρ	1025 $[kg/m^3]$
$\mathbf{r}_B$	$[0.0, 0.0, 0.0]^T$ m		
$\mathbf{r}_G^{\text{true}}$	$[0.00295, 0.00054, 0.00219]^T$ m		
$\mathbf{r}_G^{\text{adj}}$	$[0.00295, 0, 0.00219]^T$ m		

to save energy. With a corrodible wire, the weight will be released from the vehicle at the sea bottom after the wire corrodes away.

The asymmetric center of gravity of the vehicle, $\mathbf{r}_G^{\text{true}}$, in the y-axis induces spiral motion while descending. Spiral motion has been studied as one of the steady-state gliding motions for underwater gliders [17], [18]. Our previous work [15] has exploited spiral motion to estimate ocean flow as active perception and presented preliminary results on improved mid-water localization using IMU and depth sensors only. In this article, we further investigate the interplay between vehicle motion and ocean flow and develop an active perception framework for AUV navigation that exploits general vehicle motion, not limited to spiral motion. To this end, we adjust the center of gravity of DROP-Sphere from $\mathbf{r}_G^{\text{true}} = [0.00295, 0.00054, 0.00219]^T$ m to $\mathbf{r}_G^{\text{adj}} = [0.00295, 0, 0.00219]^T$ m and use $\mathbf{r}_G^{\text{adj}}$ instead of $\mathbf{r}_G^{\text{true}}$ for analysis and simulations throughout this article.

III. ACTIVE PERCEPTION FOR AUV NAVIGATION

Let us consider a vehicle with IMU and depth sensors as its primary navigational sensors. Motivated by our testbed AUV introduced in Section II-B, we consider a scenario in which this vehicle, with a drop weight attached, descends without using active propulsion due to its temporary negative buoyancy through the water column over a time interval $[t_0, t_f], t_f > t_0$ in the presence of time-varying flow. Given vehicle motion model (2) and (3), our primary goal is to estimate the vehicle state for navigation and localization using IMU and depth sensors only. In addition, simultaneously with the primary goal, we want to estimate the flow state and incorporate the estimated flow in vehicle state estimation as external information to mitigate the drift error.

In state estimation, the ability to determine the initial state of a system using knowledge of the system input and output sequences is represented by the notion of observability. For vehicle state estimation, we have a nonlinear system with vehicle motion model (2) and (3). A common tool for checking local weak observability for a nonlinear system is the observability rank condition [27], [28]. With sensor constraints, the system does not in general meet the observability rank condition. In addition, augmenting the vehicle state with the flow state will increase the complexity of state estimation.

In this section, we first introduce vehicle and flow motion models separated from the general vehicle motion model presented in Section II-A. This separation allows us to formulate our active perception problem for AUV navigation addressed in this article. A detail of the problem is provided later in this section.

A. Vehicle and Flow Motion Models: Simplification and Discretization

The vehicle dynamic model (3) can be simplified by assuming irrotational and nearly constant flow in the Earth-fixed frame (i.e., $f_\phi = f_\theta = f_\psi = 0$ and $\dot{\mathbf{f}}^I \approx 0$), which is a widely used approach in the literature (e.g., [25]). In fact, the rotational component of ocean flow is often ignored for simplification and the assumption on irrotational flow may be reasonable if a vehicle does not stay at a fixed position. However, the assumption on nearly constant flow may be valid only for spatiotemporally local regions around the initial deployment time and location of a vehicle. To account for spatiotemporal variability of flow, we consider time-varying flow as noise-driven for estimation, which is a general approach in the case with no prior knowledge of flow (e.g., [29]).

With these assumptions on the flow, flow motion in the body-fixed frame can be derived as

$$\dot{\mathbf{f}}_1 = -\mathbf{S}(\boldsymbol{\nu}_2)\mathbf{f}_1 = -\mathbf{S}(\boldsymbol{\nu}_{r2})\mathbf{f}_1 \tag{7}$$

$$\dot{\mathbf{f}}_2 = 0 \tag{8}$$

where $\mathbf{S}(\mathbf{x}) \in \mathbb{R}^{3\times3}$ is a skew-symmetric matrix defined with elements of $\mathbf{x} \in \mathbb{R}^3$ (see [25] for details of the derivation). Please note that $\boldsymbol{\nu}_2 = \boldsymbol{\nu}_{r2}$ for irrotational flow. In addition, since $\mathbf{f}_2 = 0$ and $\mathbf{f}_2^I = 0$ at all times for irrotational flow, $\mathbf{f}_2$ is omitted in our problem throughout the article. Then, the flow motion model (7) is discretized as

$$\begin{aligned}\mathbf{f}_{1,k+1} &= \mathbf{f}_{1,k} - h\mathbf{S}(\boldsymbol{\nu}_{r2,k})\mathbf{f}_{1,k} \\ &= (I - h\mathbf{S}(\boldsymbol{\nu}_{r2,k}))\mathbf{f}_{1,k} \\ &= \mathbf{F}_{\mathbf{f}_1}(\boldsymbol{\nu}_{r,k})\mathbf{f}_{1,k}\end{aligned} \tag{9}$$

where k is the time step and h is the time step size. In this article, we use the Euler method with small time step size h for discretization.

By using (7) and (8) along with a parameterization of C_{RB}, (3) can be simplified to describe vehicle motion relative to flow as

$$M\dot{\boldsymbol{\nu}}_r + C(\boldsymbol{\nu}_r)\boldsymbol{\nu}_r + D(\boldsymbol{\nu}_r)\boldsymbol{\nu}_r + \boldsymbol{\sigma}(\boldsymbol{\eta}) = \boldsymbol{\tau} \tag{10}$$

where $M = M_{\mathrm{RB}} + M_A$ and $C = C_{\mathrm{RB}} + C_A$. Then, the vehicle motion model (2) and (10) is discretized as

$$\begin{aligned}\boldsymbol{\eta}_{k+1} &= \boldsymbol{\eta}_k + hJ(\boldsymbol{\eta}_{2,k})(\boldsymbol{\nu}_{r,k} + \mathbf{f}_k) \\ &= \mathcal{F}_{\boldsymbol{\eta}}(\boldsymbol{\eta}_k, \boldsymbol{\nu}_{r,k}, \mathbf{f}_{1,k}) \qquad (11) \\ \boldsymbol{\nu}_{r,k+1} &= \boldsymbol{\nu}_{r,k} + hM^{-1}\big(\boldsymbol{\tau}_k - C(\boldsymbol{\nu}_{r,k})\boldsymbol{\nu}_{r,k} - D(\boldsymbol{\nu}_{r,k})\boldsymbol{\nu}_{r,k} \\ &\qquad - \boldsymbol{\sigma}(\boldsymbol{\eta}_k)\big) \\ &= \mathcal{F}_{\boldsymbol{\nu}_r}(\boldsymbol{\eta}_k, \boldsymbol{\nu}_{r,k}, \boldsymbol{\tau}_k) \qquad (12)\end{aligned}$$

respectively.

B. Problem Formulation

By using the vehicle and flow motion models obtained in Section III-A, we separate vehicle and flow state estimation, allowing us to employ a linear time-varying system for flow state estimation and associated uniform complete observability notion, discussed in detail in Section IV. For self-contained presentation, we restate the definition of uniform complete observability [30], [31].

Definition 1: A system, given by

$$\boldsymbol{\chi}_{k+1} = \mathbf{F}_k \boldsymbol{\chi}_k + \boldsymbol{\xi}_k^{\chi} \qquad (13)$$

$$\boldsymbol{\zeta}_k = \mathbf{H}_k \boldsymbol{\chi}_k + \boldsymbol{\xi}_k^{\zeta} \qquad (14)$$

is uniformly completely observable if there exist positive constants K, α_1, and α_2 such that

$$\alpha_1 I \leq \mathcal{G}_{\mathrm{uco}}(k, k-K) \leq \alpha_2 I \qquad (15)$$

where

$$\mathcal{G}_{\mathrm{uco}}(k, k-K) = \sum_{j=k-K}^{k} \boldsymbol{\Phi}(j,k)^T \mathbf{H}_j^T \mathbf{R}_j^{-1} \mathbf{H}_j \boldsymbol{\Phi}(j,k) \qquad (16)$$

is the observability Gramian, $\boldsymbol{\Phi}(k, j) = \mathbf{F}_{k-1}\mathbf{F}_{k-2}, \ldots, \mathbf{F}_j$ is the state transition matrix from time step j to k for $k > j$, which satisfies $\boldsymbol{\Phi}(k, j) = \boldsymbol{\Phi}(j, k)^{-1}$ and $\boldsymbol{\Phi}(k, k) = I$, and $\mathbf{R}_j$ is the covariance matrix for observation noise $\boldsymbol{\xi}^{\zeta}$ for time step j.

Due to the coupling between vehicle motion and ocean flow, observability Gramian $\mathcal{G}_{\mathrm{uco}}$ for the flow state depends on vehicle motion, which will be discussed in detail in Section IV-C. In this article, we extend our previous work [15], which exploited spiral motion, to establish more rigorous criteria pertaining to the interplay between vehicle motion and ocean flow for active perception considering general vehicle dynamics. In this context, we define the problem of active perception, i.e., to design vehicle control to improve flow estimation, for underwater navigation as follows.

Problem 1: Given observation data from IMU and depth sensors with known noise statistics, build a vehicle controller such that

$$\boldsymbol{\tau}_k^{\star} = \underset{\boldsymbol{\tau}_k}{\operatorname{argmax}}\, \mathcal{F}^{\mathrm{ap}}(\mathcal{G}_{\mathrm{uco}}(k+1, k-K+1)) \qquad (17)$$

$$\text{s.t. } (11), \quad (12) \qquad (18)$$

where (11) and (12) are the discretized vehicle motion model and $\mathcal{F}^{\mathrm{ap}}$ is the information metric regarding observability and estimation performance for active perception.

Problem 2: Given vehicle control obtained through Problem 1, design state estimators for the vehicle and flow states so that the estimated flow can help improve vehicle state estimation.

Through solving Problem 1, the optimization variable, which is the control input $\boldsymbol{\tau}_k$, is chosen such that vehicle motion maximizes $\mathcal{F}^{\mathrm{ap}}$. Please note that $\boldsymbol{\tau}_k$ is embedded in constraint (12). In this article, since we assume that our vehicle descends without active propulsion, we choose $\mathcal{F}^{\mathrm{ap}}$ only to improve flow state estimation without goal and depth constraints. The solution of Problem 1 will provide more favorable conditions to solve Problem 2. Therefore, we refer to the control strategy in Problem 1 as active perception control. The control objectives are typically mission-specific and vary by applications. If other control objectives need to be considered, we may regard active perception control as input injection as long as it is not canceled out by other control objectives. Therefore, the framework has a potential to be extended to various navigation tasks as long as the dependence of flow state observability on vehicle motion is leveraged. Details about the systems for vehicle and flow state estimation and our choices for $\mathcal{F}^{\mathrm{ap}}$ are discussed in Sections IV and V.

IV. Active Perception-Oriented System Modeling

In this section, we present the system models used for active perception. First, for vehicle and flow states governed by the corresponding motion models presented in Section III-A, individual system models for their estimation are formulated with separate observation equations based on the measurements from IMU and depth sensors. Then, flow state observability in relation to vehicle motion is discussed to show how active perception can be established using the constructed system models.

A. System Equations for Vehicle State Estimation

With the vehicle and flow motion models derived in Section III-A, let us define the vehicle state as $\boldsymbol{\chi}_{\mathbf{v}} = [\boldsymbol{\eta}^T, \boldsymbol{\nu}_r^T]^T \in \mathbb{R}^{12}$, governed by (11) and (12), and the flow state as $\boldsymbol{\chi}_{\mathbf{f}_1} = \mathbf{f}_1 \in \mathbb{R}^3$, governed by (9). While conventional state estimation approaches augment the state variable by combining the vehicle and flow states, we separate estimation of the vehicle and flow states to facilitate flow state estimation. The vehicle state equation is constructed as

$$\boldsymbol{\chi}_{\mathbf{v},k+1} = \begin{bmatrix} \mathcal{F}_{\boldsymbol{\eta}}(\boldsymbol{\chi}_{\mathbf{v},k}, \boldsymbol{\chi}_{\mathbf{f}_1,k}) \\ \mathcal{F}_{\boldsymbol{\nu}_r}(\boldsymbol{\chi}_{\mathbf{v},k}, \boldsymbol{\tau}_k) \end{bmatrix} + \boldsymbol{\xi}_k^{\chi_{\mathbf{v}}} \qquad (19)$$

where $\boldsymbol{\xi}_k^{\chi_{\mathbf{v}}} \in \mathbb{R}^{12}$ is the process noise assumed to be zero-mean Gaussian with known covariance $\mathbf{Q}_k^{\chi_{\mathbf{v}}} \in \mathbb{R}^{12\times 12}$.

In inertial navigation, the angular velocity and linear acceleration measurements from the gyroscope and accelerometer of an IMU are the fundamental data. Let $\boldsymbol{\nu}_2^{\mathrm{imu}} \in \mathbb{R}^3$ and $\dot{\boldsymbol{\nu}}_1^{\mathrm{imu.g}} \in \mathbb{R}^3$ denote the measurements from the gyroscope and accelerometer, respectively, which are expressed for time step k as

$$\boldsymbol{\nu}_{2,k}^{\mathrm{imu}} = \boldsymbol{\nu}_{2,k} + \mathbf{b}_k^{\mathrm{gyro}} + \boldsymbol{\xi}_k^{\mathrm{gyro}} \qquad (20)$$

$$\dot{\boldsymbol{\nu}}_{1,k}^{\mathrm{imu.g}} = \dot{\boldsymbol{\nu}}_{1,k} + {}_I^B R(\boldsymbol{\eta}_{2,k})\mathbf{g} + \mathbf{b}_k^{\mathrm{acc}} + \boldsymbol{\xi}_k^{\mathrm{acc}} \qquad (21)$$

where $\mathbf{b}_k^{\text{gyro}} \in \mathbb{R}^3$ and $\mathbf{b}_k^{\text{acc}} \in \mathbb{R}^3$ are biases, and $\boldsymbol{\xi}_k^{\text{gyro}} \in \mathbb{R}^3$ and $\boldsymbol{\xi}_k^{\text{acc}} \in \mathbb{R}^3$ are measurement noise described as zero-mean Gaussian with known covariance $\mathbf{R}_k^{\text{gyro}} \in \mathbb{R}^{3\times3}$ and $\mathbf{R}_k^{\text{acc}} \in \mathbb{R}^{3\times3}$, respectively. The term $\mathbf{g} = [0, 0, g]^T \in \mathbb{R}^3$ is the vector of gravity with g being the gravity of the Earth in the z-axis of the inertial frame. We obtain the vehicle linear acceleration denoted by $\dot{\boldsymbol{\nu}}_1^{\text{imu}} \in \mathbb{R}^3$ for time step k as

$$\dot{\boldsymbol{\nu}}_{1,k}^{\text{imu}} = \dot{\boldsymbol{\nu}}_{1,k}^{\text{imu.g}} - {}_I^B R(\boldsymbol{\eta}_{2,k})\mathbf{g}. \tag{22}$$

Remark 1: While the estimation of biases in the IMU measurements is widely studied and can be done by augmenting the state with the bias (e.g., [11], [12]), our proposed framework does not consider bias estimation. However, to understand the influence of bias on the proposed framework, we test the framework using simulated IMU data with bias. Suppose that a bias can be simply modeled as a summation of a constant bias term and a time-varying bias term (see Section VI-A2 for details). We assume that the constant bias term is zero for simplicity of analysis and focus on evaluating the effect of the time-varying bias term on the performance of the framework. To extend the framework to nonzero constant bias cases, a constant bias term can be augmented to the state so that it can be estimated together with the other state variables, as discussed in [11] and [12].

Remark 2: The rotation matrix ${}_I^B R$ in (22) is computed by using the estimated orientation since the true orientation is typically unknown in underwater applications. Note that the accuracy of the estimated orientation can significantly affect the accuracy of $\dot{\boldsymbol{\nu}}_1^{\text{imu}}$.

The orientation of a vehicle can be estimated using the measurement from an IMU by attitude estimation algorithms (e.g., [32]–[35]). We denote the estimated orientation by $\boldsymbol{\eta}_2^{\text{att}} \in \mathbb{R}^3$, which is expressed for time step k as

$$\boldsymbol{\eta}_{2,k}^{\text{att}} = \boldsymbol{\eta}_{2,k} + \mathbf{b}_k^{\text{att}} + \boldsymbol{\xi}_k^{\text{att}} \tag{23}$$

where $\mathbf{b}_k^{\text{att}} \in \mathbb{R}^3$ is a bias and $\boldsymbol{\xi}_k^{\text{att}} \in \mathbb{R}^3$ is the measurement noise, which includes estimation error and IMU measurement noise, described as zero-mean Gaussian with known covariance $\mathbf{R}_k^{\text{att}} \in \mathbb{R}^{3\times3}$. In addition, the measured depth, denoted by $z^{\text{depth}} \in \mathbb{R}$, is expressed for time step k as

$$z_k^{\text{depth}} = z_k + \xi_k^{\text{depth}} \tag{24}$$

where $\xi_k^{\text{depth}} \in \mathbb{R}$ is the measurement noise assumed to be zero-mean Gaussian with known covariance $R_k^{\text{depth}} \in \mathbb{R}$. Please note that in this article, we assume that the IMU and depth sensors have the same sampling frequency.

The observation vector for vehicle state estimation is constructed as $\boldsymbol{\zeta}_{\mathbf{v}} = [z^{\text{depth}}, (\boldsymbol{\eta}_2^{\text{att}})^T, (\boldsymbol{\nu}_2^{\text{imu}})^T, (\dot{\boldsymbol{\nu}}_1^{\text{imu}})^T]^T \in \mathbb{R}^{10}$. For time step k, the observation equation is given by

$$\begin{aligned}\boldsymbol{\zeta}_{\mathbf{v},k} &= \begin{bmatrix} z_k \\ \boldsymbol{\eta}_{2,k} \\ \boldsymbol{\nu}_{2,k} \\ \dot{\boldsymbol{\nu}}_{r1,k} + \dot{\mathbf{f}}_{1,k} \end{bmatrix} + \boldsymbol{\xi}_k^{\zeta_{\mathbf{v}}} \\ &= \begin{bmatrix} z_k \\ \boldsymbol{\eta}_{2,k} \\ \boldsymbol{\nu}_{2,k} \\ \dot{\boldsymbol{\nu}}_{r1,k} - \mathbf{S}(\boldsymbol{\nu}_{r2,k})\mathbf{f}_{1,k} \end{bmatrix} + \boldsymbol{\xi}_k^{\zeta_{\mathbf{v}}} \\ &= \mathcal{H}_{\mathbf{v}}(\boldsymbol{\chi}_{\mathbf{v},k}, \boldsymbol{\chi}_{\mathbf{f}_1,k}) + \boldsymbol{\xi}_k^{\zeta_{\mathbf{v}}} \end{aligned} \tag{25}$$

where measurement noise $\boldsymbol{\xi}_k^{\zeta_{\mathbf{v}}} = [\xi_k^{\text{depth}}, (\boldsymbol{\xi}_k^{\text{att}})^T, (\boldsymbol{\xi}_k^{\text{gyro}})^T, (\boldsymbol{\xi}_k^{\text{acc}})^T]^T \in \mathbb{R}^{10}$ is assumed to be zero-mean Gaussian with known covariance matrix $\mathbf{R}_k^{\zeta_{\mathbf{v}}} = \text{diag}(R_k^{\text{depth}}, \mathbf{R}_k^{\text{att}}, \mathbf{R}_k^{\text{gyro}}, \mathbf{R}_k^{\text{acc}}) \in \mathbb{R}^{10\times10}$.

B. System Equations for Flow State Estimation

Along with the system for vehicle state estimation constructed in Section IV-A, a system for flow state estimation enables our active perception framework. With vehicle state $\boldsymbol{\chi}_{\mathbf{v}}$ and flow state $\boldsymbol{\chi}_{\mathbf{f}_1}$, the flow state equation is expressed as

$$\boldsymbol{\chi}_{\mathbf{f}_1,k+1} = \mathbf{F}_{\mathbf{f}_1}(\boldsymbol{\chi}_{\mathbf{v},k})\boldsymbol{\chi}_{\mathbf{f}_1,k} + \boldsymbol{\xi}_k^{\chi_{\mathbf{f}_1}} \tag{26}$$

where $\boldsymbol{\xi}_k^{\chi_{\mathbf{f}_1}} \in \mathbb{R}^3$ is process noise represented as zero-mean Gaussian with known covariance $\mathbf{Q}_k^{\chi_{\mathbf{f}_1}} \in \mathbb{R}^{3\times3}$. From the depth sensor, the depth rate $\dot{z}^{\text{dr}} \in \mathbb{R}$ for time step k is approximated as follows:

$$\begin{aligned}\dot{z}_k^{\text{dr}} &= \dot{z}_k + \xi_k^{\text{dr}} \\ &\approx \frac{z_{k+1}^{\text{depth}} - z_k^{\text{depth}}}{h} \end{aligned} \tag{27}$$

where z_k^{depth} is the depth measurement at time step k, described by (24), and $\xi_k^{\text{dr}} \in \mathbb{R}$ is measurement noise assumed to be zero-mean Gaussian with known covariance $\mathbf{R}_k^{\text{dr}} \in \mathbb{R}$.

The observation vector for flow state estimation is constructed as $\boldsymbol{\zeta}_{\mathbf{f}_1} = [(\dot{\boldsymbol{\nu}}_1^{\text{imu}})^T, z^{\text{dr}}]^T \in \mathbb{R}^4$. For time step k, the observation equation is given by

$$\begin{aligned}\boldsymbol{\zeta}_{\mathbf{f}_1,k} &= \begin{bmatrix} \dot{\boldsymbol{\nu}}_{r1,k} + \dot{\mathbf{f}}_{1,k} \\ \dot{z}_k \end{bmatrix} + \boldsymbol{\xi}_k^{\zeta_{\mathbf{f}_1}} \\ &= \begin{bmatrix} \dot{\boldsymbol{\nu}}_{r1,k} - \mathbf{S}(\boldsymbol{\nu}_{r2,k})\mathbf{f}_{1,k} \\ [0, 0, 1] \times {}_B^I R(\boldsymbol{\eta}_{2,k})(\boldsymbol{\nu}_{r1,k} + \mathbf{f}_{1,k}) \end{bmatrix} + \boldsymbol{\xi}_k^{\zeta_{\mathbf{f}_1}} \\ &= \mathcal{H}_{\mathbf{f}_1}(\boldsymbol{\chi}_{\mathbf{v},k}, \boldsymbol{\chi}_{\mathbf{f}_1,k}) + \boldsymbol{\xi}_k^{\zeta_{\mathbf{f}_1}} \end{aligned} \tag{28}$$

where measurement noise $\boldsymbol{\xi}_k^{\zeta_{\mathbf{f}_1}} = [(\boldsymbol{\xi}_k^{\text{acc}})^T, \xi_k^{\text{dr}}]^T \in \mathbb{R}^4$ is assumed to be zero-mean Gaussian with known covariance matrix $\mathbf{R}_k^{\zeta_{f_1}} = \text{diag}(\mathbf{R}_k^{\text{acc}}, \mathbf{R}_k^{\text{dr}}) \in \mathbb{R}^{4\times4}$. While the accelerometer measurement already provides the information about the flow for all DOF in the body-fixed frame, the depth-rate measurement provides complementary information about the flow in the inertial frame. This complementarity can improve observability and state estimation, which will be discussed in Sections IV-C and VI-C.

Assuming that the vehicle state is given, we reformulate the measurement equation for the flow state (28). By subtracting the terms that depend on the vehicle state only from (28), the observation vector $\boldsymbol{\zeta}'_{\mathbf{f}_1,k}$ is defined as

$$\begin{aligned}\boldsymbol{\zeta}'_{\mathbf{f}_1,k} &= \boldsymbol{\zeta}_{\mathbf{f}_1,k} - \begin{bmatrix} \dot{\boldsymbol{\nu}}_{r1,k} \\ [0, 0, 1] \times {}_B^I R(\boldsymbol{\eta}_{2,k})\boldsymbol{\nu}_{r1,k} \end{bmatrix} \\ &= \begin{bmatrix} -\mathbf{S}(\boldsymbol{\nu}_{r2,k}) \\ [0, 0, 1] \times {}_B^I R(\boldsymbol{\eta}_{2,k}) \end{bmatrix} \mathbf{f}_{1,k} + \boldsymbol{\xi}_k^{\zeta_{\mathbf{f}_1}} \\ &= \mathbf{H}_{\mathbf{f}_1}(\boldsymbol{\chi}_{\mathbf{v},k})\boldsymbol{\chi}_{\mathbf{f}_1,k} + \boldsymbol{\xi}_k^{\zeta_{\mathbf{f}_1}}. \end{aligned} \tag{29}$$

Then, the system (26) and (29) for the flow state is a linear time-varying system, which allows us to analyze uniform complete observability for the flow state.

C. Flow State Observability and Vehicle Motion Design

For notational convenience, let $\mathbf{F}_{\mathbf{f}_1,j} = \mathbf{F}_{\mathbf{f}_1}(\boldsymbol{\chi}_{\mathbf{v},j})$ and $\mathbf{H}_{\mathbf{f}_1,j} = \mathbf{H}_{\mathbf{f}_1}(\boldsymbol{\chi}_{\mathbf{v},j})$. The observability Gramian corresponding to system (26) and (29) for flow state estimation is given by

$$\mathcal{G}^{\mathbf{f}_1}_{\text{uco}}(k, k-K) = \sum_{j=k-K}^{k} \boldsymbol{\Phi}_{\mathbf{f}_1}(j,k)^T \mathbf{H}^T_{\mathbf{f}_1,j} \left(\mathbf{R}^{\boldsymbol{\zeta}_{f_1}}_j\right)^{-1} \times \mathbf{H}_{\mathbf{f}_1,j} \boldsymbol{\Phi}_{\mathbf{f}_1}(j,k) \quad (30)$$

where $\boldsymbol{\Phi}_{\mathbf{f}_1}(k,j) = \mathbf{F}_{\mathbf{f}_1,k-1}\mathbf{F}_{\mathbf{f}_1,k-2}, \ldots, \mathbf{F}_{\mathbf{f}_1,j}$ is the state transition matrix from time step j to k, $k > j$ and $\mathbf{R}^{\boldsymbol{\zeta}_{f_1}}_j$ is the covariance matrix for noise $\boldsymbol{\xi}^{\boldsymbol{\zeta}_{\mathbf{f}_1}}$ for time step j. To satisfy the condition (15), $\mathcal{G}^{\mathbf{f}_1}_{\text{uco}}$ should be bounded and positive definite (i.e., all the eigenvalues are positive). Gramian $\mathcal{G}^{\mathbf{f}_1}_{\text{uco}}$ is bounded since $\mathbf{R}^{\boldsymbol{\zeta}_{f_1}}_j$ is bounded by design, and $\mathbf{F}_{\mathbf{f}_1,j}$ and $\mathbf{H}_{\mathbf{f}_1,j}$ are bounded since vehicle angular velocity and orientation are physically bounded. In addition, Gramian $\mathcal{G}^{\mathbf{f}_1}_{\text{uco}}$ is positive definite or positive semidefinite by its structure.

To guarantee the definiteness of $\mathcal{G}^{\mathbf{f}_1}_{\text{uco}}$, we should check for the definiteness of $\mathbf{R}^{\boldsymbol{\zeta}_{f_1}}_j$, $\mathbf{H}^T_{\mathbf{f}_1,j}\mathbf{H}_{\mathbf{f}_1,j}$, and $\boldsymbol{\Phi}_{\mathbf{f}_1}(j,k)^T\boldsymbol{\Phi}_{\mathbf{f}_1}(j,k)$. Matrix $\mathbf{R}^{\boldsymbol{\zeta}_{f_1}}_j$ is positive definite by design, and with small h and $\boldsymbol{\nu}_{r2}$, $\boldsymbol{\Phi}_{\mathbf{f}_1}(j,k)^T\boldsymbol{\Phi}_{\mathbf{f}_1}(j,k)$ is positive definite. Now, let us consider $\mathbf{H}_{\mathbf{f}_1,j}$ as a block matrix, such as

$$\mathbf{H}_{\mathbf{f}_1,j} = \begin{bmatrix} -\mathbf{S}_j \\ \mathbf{b}_j \end{bmatrix} \quad (31)$$

where matrix $\mathbf{S}_j = \mathbf{S}(\boldsymbol{\nu}_{r2,j})$ and row vector $\mathbf{b}_j = [0,0,1] \times {}^I_B R(\boldsymbol{\eta}_{2,j})$. Then, $\mathbf{H}^T_{\mathbf{f}_1,j}\mathbf{H}_{\mathbf{f}_1,j} = \mathbf{S}^T_j\mathbf{S}_j + \mathbf{b}^T_j\mathbf{b}_j$. With nonzero elements for $\mathbf{S}$, $\mathbf{S}^T_j\mathbf{S}_j$ is a positive semidefinite matrix of rank 2. Now, note that $\mathbf{b}^T_j\mathbf{b}_j$ is a rank-1 matrix. If the nonzero depth-rate measurement leads $\mathbf{b}^T_j\mathbf{b}_j$ to have a linearly independent column to $\mathbf{S}^T_j\mathbf{S}_j$, then $\mathbf{H}^T_{\mathbf{f}_1,j}\mathbf{H}_{\mathbf{f}_1,j}$ is positive definite, which shows a qualitative benefit of having the depth-rate measurement for flow state estimation. However, in case that the depth-rate measurement is not available or the depth rate is zero (e.g., a vehicle is staying at a certain depth), we have $\mathbf{b}^T_j\mathbf{b}_j = 0$ and $\mathbf{H}^T_{\mathbf{f}_1,j}\mathbf{H}_{\mathbf{f}_1,j}$ is positive semidefinite and has rank 2.

While the definiteness of each additive term $\boldsymbol{\Phi}(j,k)^T\mathbf{H}^T_j\mathbf{R}^{-1}_j\mathbf{H}_j\boldsymbol{\Phi}(j,k)$, $j \in [k-K,k]$ in $\mathcal{G}^{\mathbf{f}_1}_{\text{uco}}$, is not guaranteed, if the additive terms have three linearly independent columns, $\mathcal{G}^{\mathbf{f}_1}_{\text{uco}}$ is positive definite (i.e., all the eigenvalues of $\mathcal{G}^{\mathbf{f}_1}_{\text{uco}}$ are nonzero positive). Due to the dependence of $\mathbf{S}$ in $\mathbf{H}_{\mathbf{f}_1}$ on vehicle state $\boldsymbol{\nu}_{r2}$, vehicle motion design plays an important role to achieve observability for the flow state. In this context, we rewrite Definition 1 to adapt it for our active perception problem as follows.

Definition 2: System (26) and (29) for flow state estimation is uniformly completely observable if vehicle motion on interval $[k-K,k]$ with constant K is designed such that terms $\boldsymbol{\Phi}(j,k)^T\mathbf{H}^T_j\mathbf{R}^{-1}_j\mathbf{H}_j\boldsymbol{\Phi}(j,k)$, $j \in [k-K,k]$, lead $\mathcal{G}^{\mathbf{f}_1}_{\text{uco}}$ to have three linearly independent columns (i.e., to have full rank).

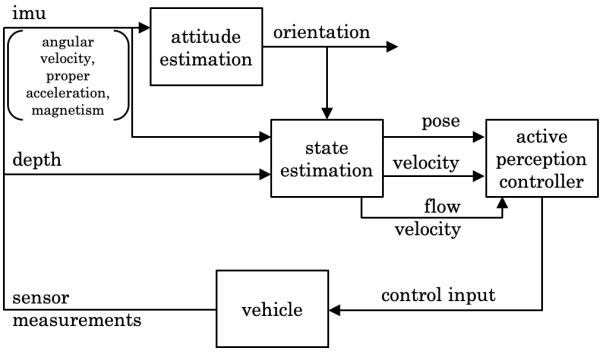

Fig. 4. Schematic of our approach.

V. Active Perception Framework for AUV Navigation Under Sensor Constraints

In this section, we propose our active perception framework for AUV navigation. First, we introduce information metrics used as $\mathcal{F}^{\text{ap}}$. Then, we present our framework, including active perception control and state estimation strategies. The structure of the proposed framework is shown in Fig. 4.

A. Information Metrics for Active Perception

As widely known (e.g., [30], [31]), observability Gramian $\mathcal{G}_{\text{uco}}$ is an information matrix, that is, for system (26) and (29), $\mathcal{G}_{\text{uco}}$ describes the informational difference with respect to the variation of the vehicle state $\boldsymbol{\nu}_{r2}$ (i.e., vehicle motion). Instead of the matrix form, scalar measures of information metrics have been preferred in optimization. Please refer to [36] and [37] for an overview of scalar measures of information metrics. Among many scalar measures, $(1/\lambda_{\min}(\cdot))$, where $\lambda_{\min}(\cdot)$ denotes the smallest eigenvalue of $(\cdot)$, represents the maximum variance of the estimate. Therefore, we choose

$$\mathcal{F}^{\text{ap}}_1 = \lambda_{\min}\left(\mathcal{G}^{\mathbf{f}_1}_{\text{uco}}(k+1,k)\right) \quad (32)$$

as an information metric for active perception, that is, solving the optimization problem in (17) with $\mathcal{F}^{\text{ap}} = \mathcal{F}^{\text{ap}}_1$ generates vehicle control input such that vehicle motion maximizes the information with respect to vehicle motion and minimizes the maximum variance of the estimate.

As stated in Section IV-B, having the depth-rate measurement may provide qualitative benefit for flow state estimation, leading $\mathbf{H}^T_{\mathbf{f}_1,k}\mathbf{H}_{\mathbf{f}_1,k}$ to become full rank. In this section, to consider more general cases for analysis purposes, we suppose that $\mathbf{H}^T_{\mathbf{f}_1,k}\mathbf{H}_{\mathbf{f}_1,k}$ is a positive semidefinite matrix of rank 2, which represents active perception without the depth-rate measurement or with zero depth rate (i.e., a constant depth is maintained).

By definition, we have

$$\mathcal{G}^{\mathbf{f}_1}_{\text{uco}}(k+1,k) = \sum_{j=k}^{k+1} \boldsymbol{\Phi}_{\mathbf{f}_1}(j,k+1)^T \mathbf{H}^T_{\mathbf{f}_1,j} \left(\mathbf{R}^{\boldsymbol{\zeta}_{f_1}}_j\right)^{-1} \times \mathbf{H}_{\mathbf{f}_1,j} \boldsymbol{\Phi}_{\mathbf{f}_1}(j,k+1) \quad (33)$$

which can be expanded as

$$\mathcal{G}^{\mathbf{f}_1}_{\text{uco}}(k+1,k) = \mathbf{F}^T_{\mathbf{f}_1,k}\mathbf{H}^T_{\mathbf{f}_1,k}\left(\mathbf{R}^{\boldsymbol{\zeta}_{f_1}}_k\right)^{-1}\mathbf{H}_{\mathbf{f}_1,k}\mathbf{F}_{\mathbf{f}_1,k} + \mathbf{H}^T_{\mathbf{f}_1,k+1}\left(\mathbf{R}^{\boldsymbol{\zeta}_{f_1}}_{k+1}\right)^{-1}\mathbf{H}_{\mathbf{f}_1,k+1} \quad (34)$$

where we used $\mathbf{\Phi}_{\mathbf{f}_\mathrm{l}}(k,k+1)=\mathbf{F}_{\mathbf{f}_\mathrm{l},k}$ and $\mathbf{\Phi}_{\mathbf{f}_\mathrm{l}}(k+1,k+1)=I$. Note that each term on the right-hand side of (34) is positive semidefinite and has rank 2, implying that each term has two linearly independent columns (i.e., $\lambda_{\min}$ of each term is zero). Since the vehicle state for time step k, $\boldsymbol{\chi}_{\mathbf{v},k}$, is given, the first term on the right-hand side of (34) is constant. On the contrary, the second term varies as the vehicle state for time step $k+1$, $\boldsymbol{\chi}_{\mathbf{v},k+1}$, changes by control input $\boldsymbol{\tau}_k$. By leveraging this point for active perception control using (32), we introduce the following theorem.

Theorem 1: System (26) and (29) is uniformly completely observable if vehicle motion is generated by control input that solves the following optimization problem:

$$\boldsymbol{\tau}_k^\star = \underset{\boldsymbol{\tau}_k}{\operatorname{argmax}}\, \lambda_{\min}\big(\mathcal{G}_{\mathrm{uco}}^{\mathbf{f}_\mathrm{l}}(k+1,k)\big) \tag{35}$$

$$\text{s.t. (11)}, \quad \text{(12)}. \tag{36}$$

Proof: Without loss of generality, we can assume that $\dot{z}_k^{\mathrm{dr}}=0$ and $\mathbf{R}_k^{\zeta_{f_\mathrm{l}}}=I$. Then, to simplify the analysis for the linearly independent columns of $\mathcal{G}_{\mathrm{uco}}^{\mathbf{f}_\mathrm{l}}(k+1,k)$ in (34), let us consider

$$\hat{\mathcal{G}}(k+1,k)=\mathbf{F}_{\mathbf{f}_\mathrm{l},k}^T\mathbf{H}_{\mathbf{f}_\mathrm{l},k}^T\mathbf{H}_{\mathbf{f}_\mathrm{l},k}\mathbf{F}_{\mathbf{f}_\mathrm{l},k}+\mathbf{H}_{\mathbf{f}_\mathrm{l},k+1}^T\mathbf{H}_{\mathbf{f}_\mathrm{l},k+1}. \tag{37}$$

Suppose that $\boldsymbol{\tau}_k=\mathbf{0}$ and vehicle state $\boldsymbol{\nu}_{r2}$ does not change such that $\boldsymbol{\nu}_{r2,k}=[a_1,a_2,a_3]^T$ and $\boldsymbol{\nu}_{r2,k+1}=[a_1,a_2,a_3]^T$. Then, the reduced row echelon form of $\hat{\mathcal{G}}(k+1,k)$ is

$$\begin{bmatrix} 1 & 0 & -\dfrac{a_1}{a_3} \\ 0 & 1 & -\dfrac{a_2}{a_3} \\ 0 & 0 & 0 \end{bmatrix} \tag{38}$$

implying that $\lambda_{\min}[\mathcal{G}_{\mathrm{uco}}^{\mathbf{f}_\mathrm{l}}(k+1,k)]=0$. In fact, since we can simply let $\mathbf{H}_{\mathbf{f}_\mathrm{l},k}=-\mathbf{S}(\boldsymbol{\nu}_{r2,k})$ without the depth-rate measurement and we have $\mathbf{F}_{\mathbf{f}_\mathrm{l},k}=[I-h\mathbf{S}(\boldsymbol{\nu}_{r2,k})]$, the first and second terms on the right-hand side of (34) become merely products of $\mathbf{S}(\boldsymbol{\nu}_{r2,k})$; therefore, they have the same linearly independent columns. Suppose that $\boldsymbol{\tau}_k\neq\mathbf{0}$ and vehicle state $\boldsymbol{\nu}_{r2}$ changes such that $\boldsymbol{\nu}_{r2,k}=[a_1,a_2,a_3]^T$ and $\boldsymbol{\nu}_{r2,k+1}=[b_1,b_2,b_3]^T$. Then, the reduced row echelon form of $\hat{\mathcal{G}}(k+1,k)$ is an identity matrix, implying that $\lambda_{\min}[\mathcal{G}_{\mathrm{uco}}^{\mathbf{f}_\mathrm{l}}(k+1,k)]\neq 0$. Through solving (35) and (36) such that $\lambda_{\min}[\mathcal{G}_{\mathrm{uco}}^{\mathbf{f}_\mathrm{l}}(k+1,k)]$ is maximized, $\boldsymbol{\tau}_k^\star$ varies vehicle state $\boldsymbol{\nu}_{r2}$ so that the second term on the right-hand side of (34) has a linearly independent column to the first term, leading $\mathcal{G}_{\mathrm{uco}}^{\mathbf{f}_\mathrm{l}}(k+1,k)$ to have full rank. This proves the theorem. □

In addition to observability, another measure relevant to state estimation is constructability, which represents the ability of determining the current state of a system using knowledge of the system input and output sequences. (Note that constructability is a property related to observability rather than controllability.) For system (26) and (29), the constructability can be determined by using the constructability Gramian [38], which is given by

$$\mathcal{G}_{\mathrm{c}}^{\mathbf{f}_\mathrm{l}}(0,k)=\sum_{j=0}^{k}\mathbf{\Phi}_{\mathbf{f}_\mathrm{l}}(j,k)^T\mathbf{H}_{\mathbf{f}_\mathrm{l},j}^T\left(\mathbf{R}_j^{\zeta_{f_\mathrm{l}}}\right)^{-1}\times\mathbf{H}_{\mathbf{f}_\mathrm{l},j}\mathbf{\Phi}_{\mathbf{f}_\mathrm{l}}(j,k). \tag{39}$$

Note that if $K=k$ in (30) for all k, $\mathcal{G}_{\mathrm{c}}^{\mathbf{f}_\mathrm{l}}$ and $\mathcal{G}_{\mathrm{uco}}^{\mathbf{f}_\mathrm{l}}$ could be interchangeable. However, since K in (30) should be constant, they are not equivalent.

To see the explicit relationship between $\mathcal{G}_{\mathrm{c}}^{\mathbf{f}_\mathrm{l}}$ and $\mathcal{G}_{\mathrm{uco}}^{\mathbf{f}_\mathrm{l}}$, let us consider the following partition of (39):

$$\begin{aligned}\mathcal{G}_{\mathrm{c}}^{\mathbf{f}_\mathrm{l}}(0,k)=&\sum_{j=0}^{k-K-1}\mathbf{\Phi}_{\mathbf{f}_\mathrm{l}}(j,k)^T\mathbf{H}_{\mathbf{f}_\mathrm{l},j}^T\left(\mathbf{R}_j^{\zeta_{f_\mathrm{l}}}\right)^{-1}\mathbf{H}_{\mathbf{f}_\mathrm{l},j}\mathbf{\Phi}_{\mathbf{f}_\mathrm{l}}(j,k)\\&+\sum_{j=k-K}^{k}\mathbf{\Phi}_{\mathbf{f}_\mathrm{l}}(j,k)^T\mathbf{H}_{\mathbf{f}_\mathrm{l},j}^T\left(\mathbf{R}_j^{\zeta_{f_\mathrm{l}}}\right)^{-1}\mathbf{H}_{\mathbf{f}_\mathrm{l},j}\mathbf{\Phi}_{\mathbf{f}_\mathrm{l}}(j,k).\end{aligned} \tag{40}$$

Note that the second term on the right-hand side of the equation is identical to $\mathcal{G}_{\mathrm{uco}}^{\mathbf{f}_\mathrm{l}}(k,k-K)$ in (30). Since $\mathbf{\Phi}_{\mathbf{f}_\mathrm{l}}(j,k)=\mathbf{\Phi}_{\mathbf{f}_\mathrm{l}}(j,k-K-1)\mathbf{\Phi}_{\mathbf{f}_\mathrm{l}}(k-K-1,k)$, we can rewrite (40) as

$$\begin{aligned}\mathcal{G}_{\mathrm{c}}^{\mathbf{f}_\mathrm{l}}(0,k)=&\,\mathbf{\Phi}_{\mathbf{f}_\mathrm{l}}(k-K-1,k)^T\mathcal{G}_{\mathrm{c}}^{\mathbf{f}_\mathrm{l}}(0,k-K-1)\\&\times\mathbf{\Phi}_{\mathbf{f}_\mathrm{l}}(k-K-1,k)+\mathcal{G}_{\mathrm{uco}}^{\mathbf{f}_\mathrm{l}}(k,k-K).\end{aligned} \tag{41}$$

In other words, $\mathcal{G}_{\mathrm{c}}^{\mathbf{f}_\mathrm{l}}$ can be interpreted as a function of $\mathcal{G}_{\mathrm{uco}}^{\mathbf{f}_\mathrm{l}}$ with additional past information of constructability translated for time step k. This shows that $\mathcal{G}_{\mathrm{uco}}^{\mathbf{f}_\mathrm{l}}$ and $\mathcal{G}_{\mathrm{c}}^{\mathbf{f}_\mathrm{l}}$ are connected in terms of uniform complete observability.

For implementation of $\mathcal{G}_{\mathrm{c}}^{\mathbf{f}_\mathrm{l}}$, we first consider $\mathcal{G}_{\mathrm{c}}^{\mathbf{f}_\mathrm{l}}(-\infty,0)$ as the constructability Gramian for time step $k=0$ evaluated by using prior knowledge. Then, for $k=1$, we have

$$\begin{aligned}\mathcal{G}_{\mathrm{c}}^{\mathbf{f}_\mathrm{l}}(-\infty,1)=&\,\mathbf{\Phi}_{\mathbf{f}_\mathrm{l}}(0,1)^T\mathcal{G}_{\mathrm{c}}^{\mathbf{f}_\mathrm{l}}(-\infty,0)\mathbf{\Phi}_{\mathbf{f}_\mathrm{l}}(0,1)\\&+\mathbf{H}_{\mathbf{f}_\mathrm{l},1}^T\left(\mathbf{R}_1^{\zeta_{f_\mathrm{l}}}\right)^{-1}\mathbf{H}_{\mathbf{f}_\mathrm{l},1}.\end{aligned} \tag{42}$$

By recursively evaluating $\mathcal{G}_{\mathrm{c}}^{\mathbf{f}_\mathrm{l}}$, we have

$$\begin{aligned}\mathcal{G}_{\mathrm{c}}^{\mathbf{f}_\mathrm{l}}(-\infty,k+1)=&\sum_{j=-\infty}^{k+1}\mathbf{\Phi}_{\mathbf{f}_\mathrm{l}}(j,k+1)^T\mathbf{H}_{\mathbf{f}_\mathrm{l},j}^T(\mathbf{R}_j^{\zeta_{f_\mathrm{l}}})^{-1}\\&\times\mathbf{H}_{\mathbf{f}_\mathrm{l},j}\mathbf{\Phi}_{\mathbf{f}_\mathrm{l}}(j,k+1)\end{aligned} \tag{43}$$

$$\begin{aligned}=&\,\mathbf{\Phi}_{\mathbf{f}_\mathrm{l}}(k,k+1)^T\mathcal{G}_{\mathrm{c}}^{\mathbf{f}_\mathrm{l}}(-\infty,k)\mathbf{\Phi}_{\mathbf{f}_\mathrm{l}}(k,k+1)\\&+\mathbf{H}_{\mathbf{f}_\mathrm{l},k+1}^T\left(\mathbf{R}_{k+1}^{\zeta_{f_\mathrm{l}}}\right)^{-1}\mathbf{H}_{\mathbf{f}_\mathrm{l},k+1}.\end{aligned} \tag{44}$$

Along with $\mathcal{F}_1^{\mathrm{ap}}$, we also choose

$$\mathcal{F}_2^{\mathrm{ap}}=\lambda_{\min}\big(\mathcal{G}_{\mathrm{c}}^{\mathbf{f}_\mathrm{l}}(-\infty,k+1)\big) \tag{45}$$

as the second information metric for active perception. For active perception control using (45), we introduce the following theorem.

Theorem 2: System (26) and (29) is uniformly completely observable if vehicle motion is generated by control input that solves the following optimization problem:

$$\boldsymbol{\tau}_k^\star = \underset{\boldsymbol{\tau}_k}{\operatorname{argmax}}\, \lambda_{\min}\big(\mathcal{G}_{\mathrm{c}}^{\mathbf{f}_\mathrm{l}}(-\infty,k+1)\big) \tag{46}$$

$$\text{s.t. (11)}, \quad \text{(12)}. \tag{47}$$

Proof: If $\mathcal{G}_{\mathrm{c}}^{\mathbf{f}_\mathrm{l}}(-\infty,0)$ in (42) is designed as positive definite, $\mathcal{G}_{\mathrm{c}}^{\mathbf{f}_\mathrm{l}}(-\infty,k)$ is always positive definite over all k regardless of $\boldsymbol{\tau}_k$. If $\mathcal{G}_{\mathrm{c}}^{\mathbf{f}_\mathrm{l}}(-\infty,0)$ is designed as positive semidefinite, vehicle control $\boldsymbol{\tau}_k$ helps achieve uniform complete observability. Without loss of generality, assume that $\dot{z}_k^{\mathrm{dr}}=0$

and $\mathbf{R}_k^{\zeta_{f_1}} = I$. For an arbitrary $\mathcal{G}_c^{\mathbf{f}_1}(-\infty, 0)$, $\mathcal{G}_c^{\mathbf{f}_1}(-\infty, k+1)$ for time step $k = 1$ is

$$\mathcal{G}_c^{\mathbf{f}_1}(-\infty, 2) = \mathbf{\Phi}_{\mathbf{f}_1}(1,2)^T \mathcal{G}_c^{\mathbf{f}_1}(-\infty, 1)\mathbf{\Phi}_{\mathbf{f}_1}(1,2) + \mathbf{H}_{\mathbf{f}_1,2}^T \mathbf{H}_{\mathbf{f}_1,2} \tag{48}$$

$$= \mathbf{\Phi}_{\mathbf{f}_1}(1,2)^T \Big(\mathbf{\Phi}_{\mathbf{f}_1}(0,1)^T \mathcal{G}_c^{\mathbf{f}_1}(-\infty, 0)\mathbf{\Phi}_{\mathbf{f}_1}(0,1) + \mathbf{H}_{\mathbf{f}_1,1}^T \mathbf{H}_{\mathbf{f}_1,1} \Big) \mathbf{\Phi}_{\mathbf{f}_1}(1,2) + \mathbf{H}_{\mathbf{f}_1,2}^T \mathbf{H}_{\mathbf{f}_1,2} \tag{49}$$

$$= \mathbf{\Phi}_{\mathbf{f}_1}(0,2)^T \mathcal{G}_c^{\mathbf{f}_1}(-\infty, 0)\mathbf{\Phi}_{\mathbf{f}_1}(0,2) + \mathbf{\Phi}_{\mathbf{f}_1}(1,2)^T \times \mathbf{H}_{\mathbf{f}_1,1}^T \mathbf{H}_{\mathbf{f}_1,1} \mathbf{\Phi}_{\mathbf{f}_1}(1,2) + \mathbf{H}_{\mathbf{f}_1,2}^T \mathbf{H}_{\mathbf{f}_1,2}. \tag{50}$$

Note that the last two terms in (50) is $\hat{\mathcal{G}}(2,1)$ as defined in (37) in the proof for Theorem 1. Now, for arbitrary k, it is easy to see that $\mathcal{G}_c^{\mathbf{f}_1}(-\infty, k+1)$ includes $\hat{\mathcal{G}}(k+1, k)$. Therefore, the proof follows the same steps to those in the proof for Theorem 1. This proves the theorem. □

In Section V-B, we describe our design of active perception control and state estimation using these metrics. Then, the performance comparison between control strategies in Theorems 1 and 2 will be provided in Section VI.

B. Active Perception Control and State Estimation

Although Theorems 1 and 2 do not show the degree of observability, note that as discussed earlier, $(1/\lambda_{\min}(\cdot))$ represents the maximum variance of the estimate, that is, through control strategies in Theorems 1 and 2, vehicle control is chosen such that vehicle motion minimizes the maximum variance of the estimate while maintaining uniform complete observability for the flow state estimation. With either one of $\mathcal{F}_i^{\text{ap}}$, $i = \{1, 2\}$ chosen as the information metric, we design active perception control as follows:

$$\boldsymbol{\tau}_k^\star = \underset{\boldsymbol{\tau}_k}{\text{argmax}}\, \mathcal{F}_i^{\text{ap}} \tag{51}$$

$$\text{s.t. (11)}, \quad \text{(12)}. \tag{52}$$

While in motion with the active perception control, the vehicle and flow states are simultaneously estimated and the estimate of each state is used as constant for estimation of the other state. For notational convenience, let $\mathbf{F}_{\mathbf{f}_1,k} = \mathbf{F}_{\mathbf{f}_1}(\boldsymbol{\chi}_{\mathbf{v},k})$ and $\mathbf{H}_{\mathbf{f}_1,k} = \mathbf{H}_{\mathbf{f}_1}(\boldsymbol{\chi}_{\mathbf{v},k})$ since they are evaluated by using the estimate of $\boldsymbol{\chi}_{\mathbf{v},k}$. With the system in (26) and (29), the Kalman filter for flow state estimation can be derived as

$$\hat{\boldsymbol{\chi}}_{\mathbf{f}_1,k}^- = \mathbf{F}_{\mathbf{f}_1,k} \hat{\boldsymbol{\chi}}_{\mathbf{f}_1,k-1}^+ \tag{53}$$

$$\mathbf{P}_k^- = \mathbf{F}_{\mathbf{f}_1,k} \mathbf{P}_{k-1}^+ (\mathbf{F}_{\mathbf{f}_1,k})^T + \mathbf{Q}_{k-1}^{\boldsymbol{\chi}_{\mathbf{f}_1}} \tag{54}$$

$$\mathbf{K}_k = \mathbf{P}_k^- (\mathbf{H}_{\mathbf{f}_1,k})^T \Big(\mathbf{H}_{\mathbf{f}_1,k} \mathbf{P}_k^- (\mathbf{H}_{\mathbf{f}_1,k})^T + \mathbf{R}_k^{\zeta_{f_1}} \Big)^{-1} \tag{55}$$

$$\hat{\boldsymbol{\chi}}_{\mathbf{f}_1,k}^+ = \hat{\boldsymbol{\chi}}_{\mathbf{f}_1,k}^- + \mathbf{K}_k \big(\boldsymbol{\zeta}'_{\mathbf{f}_1,k} - \mathbf{H}_{\mathbf{f}_1,k} \hat{\boldsymbol{\chi}}_{\mathbf{f}_1,k}^- \big) \tag{56}$$

$$\mathbf{P}_k^+ = (I - \mathbf{K}_k \mathbf{H}_{\mathbf{f}_1,k}) \mathbf{P}_k^- (I - \mathbf{K}_k \mathbf{H}_{\mathbf{f}_1,k})^T + \mathbf{K}_k \mathbf{R}_k^{\zeta_{f_1}} \mathbf{K}_k^T \tag{57}$$

where $\hat{\boldsymbol{\chi}}_{\mathbf{f}_1,k}$ is the optimal estimate of $\boldsymbol{\rho}_k$, $(\cdot)^-$ is *a priori* of the estimate, and $\boldsymbol{\rho}_k$, $(\cdot)^+$ is *a posteriori* of the estimate. The terms $\mathbf{P}_k$ and $\mathbf{K}_k$ are the error covariance matrix and the Kalman gain, respectively. In the following theorem, we prove the convergence of the designed Kalman filter for flow state estimation.

Theorem 3: The designed Kalman filter for system (26) and (29) with control input generated by (51) and (52) is uniformly asymptotically stable.

Proof: System (26) and (29) with control input generated by (51) and (52) is uniformly completely observable by Theorems 1 and 2. Then, the proof follows directly from [30, Th. 4] or [31, Th. 7.4]. This proves the theorem. □

Remark 3: If the state is augmented with the vehicle and flow states, observability is not guaranteed for a system with IMU and depth sensor measurements. By designing a separate flow state estimator, the flow state becomes observable and the estimate of the flow state can be used to improve vehicle state estimation.

For vehicle state estimation, we use the particle filter, which is popular for the state estimation of nonlinear systems. Let $\boldsymbol{\chi}_{\mathbf{v},0:k} = \{\boldsymbol{\chi}_{\mathbf{v},0}, \ldots, \boldsymbol{\chi}_{\mathbf{v},k}\}$ and $\boldsymbol{\zeta}_{\mathbf{v},0:k} = \{\boldsymbol{\zeta}_{\mathbf{v},0}, \ldots, \boldsymbol{\zeta}_{\mathbf{v},k}\}$. The particle filter computes an approximation of the posterior density $p(\boldsymbol{\chi}_{\mathbf{v},k} | \boldsymbol{\zeta}_{\mathbf{v},0:k})$ for system (19) and (25). At each time step k, N particles are first sampled from the proposal distribution, denoted by π, such that

$$\boldsymbol{\chi}_{\mathbf{v},k}^i \sim \pi(\boldsymbol{\chi}_{\mathbf{v},k} | \boldsymbol{\chi}_{\mathbf{v},0:k-1}, \boldsymbol{\zeta}_{\mathbf{v},0:k}), \quad i = \{1, \ldots, N\}. \tag{58}$$

The proposal distribution is used instead of the true posterior $p(\boldsymbol{\chi}_{\mathbf{v},k} | \boldsymbol{\zeta}_{\mathbf{v},0:k})$, which is in general impossible to obtain. We use the vehicle state equation (19) evaluated with the estimate of $\boldsymbol{\chi}_{\mathbf{f}_1,k}$ as the proposal distribution [i.e., $\pi(\boldsymbol{\chi}_{\mathbf{v},k}^i | \boldsymbol{\chi}_{\mathbf{v},0:k-1}, \boldsymbol{\zeta}_{\mathbf{v},0:k}) = p(\boldsymbol{\chi}_{\mathbf{v},k}^i | \boldsymbol{\chi}_{\mathbf{v},k-1}^i)$]. Then, the importance weights are updated as

$$\hat{w}_k^i = w_{k-1}^i \frac{p(\boldsymbol{\zeta}_{\mathbf{v},k} | \boldsymbol{\chi}_{\mathbf{v},k}^i) p(\boldsymbol{\chi}_{\mathbf{v},k}^i | \boldsymbol{\chi}_{\mathbf{v},k-1}^i)}{\pi(\boldsymbol{\chi}_{\mathbf{v},k}^i | \boldsymbol{\chi}_{\mathbf{v},0:k-1}, \boldsymbol{\zeta}_{\mathbf{v},0:k})} \tag{59}$$

$$= w_{k-1}^i p(\boldsymbol{\zeta}_{\mathbf{v},k} | \boldsymbol{\chi}_{\mathbf{v},k}^i), \quad i = \{1, \ldots, N\} \tag{60}$$

and normalized as

$$w_k^i = \frac{\hat{w}_k^i}{\sum_{j=1}^N \hat{w}_k^{(j)}}, \quad i = \{1, \ldots, N\}. \tag{61}$$

Finally, the effective number of particles is estimated as

$$\hat{N}_{eff} = \frac{1}{\sum_{i=1}^N \big(w_k^i\big)^2} \tag{62}$$

which reflects the variance of the weights. If the effective number of particles is less than a given threshold as $\hat{N}_{\text{eff}} < N_{\text{thr}}$, then particles are resampled.

Algorithm 1 shows the procedure of our active perception design for estimation of the vehicle and flow states.

VI. Simulations

In this section, we validate our proposed framework through simulations. First, we briefly introduce our simulation setup pertaining to the environment, the IMU, and the case study scenario of vehicle descent motivated by DROP-Sphere. Under this simulation setup, we evaluate two baseline approaches followed by four implementations of the proposed framework for the case study. We provide our analysis on the proposed framework with comparison to the baseline approaches.

Algorithm 1 Vehicle and Flow State Estimation Through Active Perception

Input: Measurements from IMU and depth sensors
Output: Estimated vehicle and flow states

$k = 0$.
Initialize the vehicle state $\boldsymbol{\chi}_{\mathbf{v},0}$ and the flow state $\boldsymbol{\chi}_{\mathbf{f}_{1,0}}$.
Sample N particles for the vehicle state $\boldsymbol{\chi}^i_{\mathbf{v},0} \sim \mathcal{N}(\boldsymbol{\chi}_{\mathbf{v},0}, \Sigma_{\mathbf{v}})$, $i = \{1, \cdots, N\}$ and initialize importance weights w^i_0 for each particle.
repeat
▷ Active Perception Control
$\boldsymbol{\tau}_k \leftarrow$ (51)
▷ Measurement Update
$\boldsymbol{\zeta}_{\mathbf{v},k} \leftarrow$ (25)
$\boldsymbol{\zeta}'_{\mathbf{f},k} \leftarrow$ (29) with $\hat{\boldsymbol{\chi}}^-_{\mathbf{v},k}$
▷ Kalman Filter Correction for the Flow State
$\hat{\boldsymbol{\chi}}^+_{\mathbf{f}_1,k} \leftarrow$ (56) with $\hat{\boldsymbol{\chi}}^-_{\mathbf{v},k}$
$\mathbf{P}^+_k \leftarrow$ (57)
▷ Particle Filter Correction for the Vehicle State
$w^i_k \leftarrow$ (60), (61) with $\hat{\boldsymbol{\chi}}^+_{\mathbf{f}_1,k}$, $\boldsymbol{\tau}_k$, $i = \{1, \cdots, N\}$
$\hat{\boldsymbol{\chi}}^+_{\mathbf{v},k} \leftarrow \frac{\sum_{i=1}^N \boldsymbol{\chi}^i_{\mathbf{v},k} w^i_k}{\sum_{i=1}^N w^i_k}$
$\hat{N}_{\text{eff}} \leftarrow$ (62)
if $\hat{N}_{\text{eff}} < N_{\text{thr}}$ **then**
$\boldsymbol{\chi}^i_{\mathbf{v},k} \leftarrow$ Resampling(), $i = \{1, \cdots, N\}$
end if
▷ Particle Filter Prediction for the Vehicle State
$\boldsymbol{\chi}^i_{\mathbf{v},k+1} \leftarrow$ (19), (25) with $\hat{\boldsymbol{\chi}}^+_{\mathbf{f}_1,k}$, $\boldsymbol{\tau}_k$, $i = \{1, \cdots, N\}$
$\hat{\boldsymbol{\chi}}^-_{\mathbf{v},k+1} \leftarrow \frac{\sum_{i=1}^N \boldsymbol{\chi}^i_{\mathbf{v},k+1} w^i_k}{\sum_{i=1}^N w^i_k}$
▷ Kalman Filter Prediction for the Flow State
$\hat{\boldsymbol{\chi}}^-_{\mathbf{f}_1,k+1} \leftarrow$ (53) with $\hat{\boldsymbol{\chi}}^+_{\mathbf{v},k}$
$\mathbf{P}^-_{k+1} \leftarrow$ (54)
$\mathbf{K}_{k+1} \leftarrow$ (55)
▷ Time Step Index Update
$k = k + 1$.
until navigation is complete

A. Simulation Setup

1) Simulation Environment: We simulate environmental flow by using a two-dimensional (2-D) double-gyre pattern that occurs often in geophysical flow [39]. For horizontal position $\mathbf{r} = [x, y]^T$ and time t, a double-gyre flow field over $(x, y) \in [0, 2] \times [0, 1]$ can be described by the stream function

$$\Xi(\mathbf{r}, t) = \mathcal{A} \sin(\pi \xi(x, t)) \sin(\pi y) \tag{63}$$

where $\xi(x, t) = \alpha(t)x^2 + \beta(t)x$, $\alpha(t) = \epsilon \sin(\omega t)$, and $\beta(t) = 1 - 2\epsilon \sin(\omega t)$. The parameter $\mathcal{A}$ determines the magnitude of the flow velocity in the field, ω is the frequency of oscillation, and ϵ determines approximately how far the separation line at $x = 1$ between the two gyres moves to the left or right. Then, the velocity field is given by

$$f_x = -\frac{\partial \Xi}{\partial y} = -\pi \mathcal{A} \sin(\pi \xi(x)) \cos(\pi y) \tag{64}$$

$$f_y = \frac{\partial \Xi}{\partial x} = \pi \mathcal{A} \cos(\pi \xi(x)) \sin(\pi y) \frac{d\xi}{dx}. \tag{65}$$

The flow is time-invariant if $\epsilon = 0$, and otherwise, the gyres periodically expand and contract side to side along the x-axis within the domain. In this article, we use $\epsilon = 0.3$, $\mathcal{A} = (0.1/\pi)$, $\omega = (2\pi/T)$, and $T = 24$ h, and then rescale and translate the domain to $[-7500 \text{ m}, 12500 \text{ m}] \times [-7500 \text{ m}, 2500 \text{ m}]$ (see Fig. 5). With these parameters, the gyres move side to side by approximately 3 km in both directions every 24 h and the maximum flow velocity is approximately 0.1 m/s. We extend this 2-D flow to the 3-D space by assuming a uniform field along the z-axis (i.e., $f_z = 0$), and our proposed framework estimates the 3-D flow.

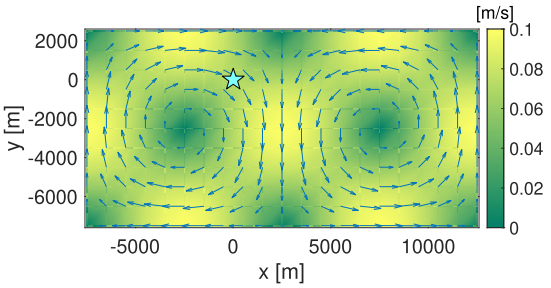

Fig. 5. Time-varying double-gyre flow field. The arrows and the surface color represent the flow and its magnitude, respectively. The colorbar on the right displays the scale of the flow. The cyan pentagram represents the deployment location of a simulated vehicle.

TABLE III
Simulated IMU Properties Based on Xsens MTi-30

Property	Gyroscope	Accelerometer
Measurement range	$\pm 450\ ^\circ/s$	$\pm 196\ m/s^2$
Constant bias	$0\ ^\circ/s$	$0\ m/s^2$
Noise density	$0.03\ ^\circ/s/\sqrt{Hz}$	$0.588 \times 10^{-3}\ m/s^2/\sqrt{Hz}$
Bias instability	$18\ ^\circ/h$	$0.147 \times 10^{-3}\ m/s^2$

2) IMU Simulation: The IMU sensor is simulated using the IMU simulation model provided in MATLAB based on the noise properties of Xsens MTi-30 used by DROP-Sphere (see Table III). In our analysis, we set the sampling frequency of the IMU as 100 Hz. Please note that while assuming zero constant bias for simplicity, we simulate an IMU with time-varying bias, described by bias instability in Table III, to see its influence on the proposed framework. In fact, the bias instability properties of Xsens MTi-30 may not be trivial and may affect the performance of our proposed framework significantly.

To analyze the noise properties in the IMU measurements, we simulate a vehicle descending through a water column without control input. Fig. 6 shows the true angular velocity and linear acceleration of the simulated vehicle, and its noisy angular velocity and linear acceleration obtained from simulated IMU measurements. From this simulation, we calculate the mean and variance of the noise in the angular velocity and linear acceleration measurements (see Table IV). These statistical values are used for our state estimator design in simulations. For attitude estimation from the IMU measurements, we use a complementary filter provided by MATLAB (see Fig. 7).

3) Vehicle Descent Scenario: In the simulation environment introduced in Section VI-A1, we deploy a virtual vehicle modeled based on our testbed AUV, described in Section II-B, with a drop weight of 0.3 kg attached. This drop weight makes

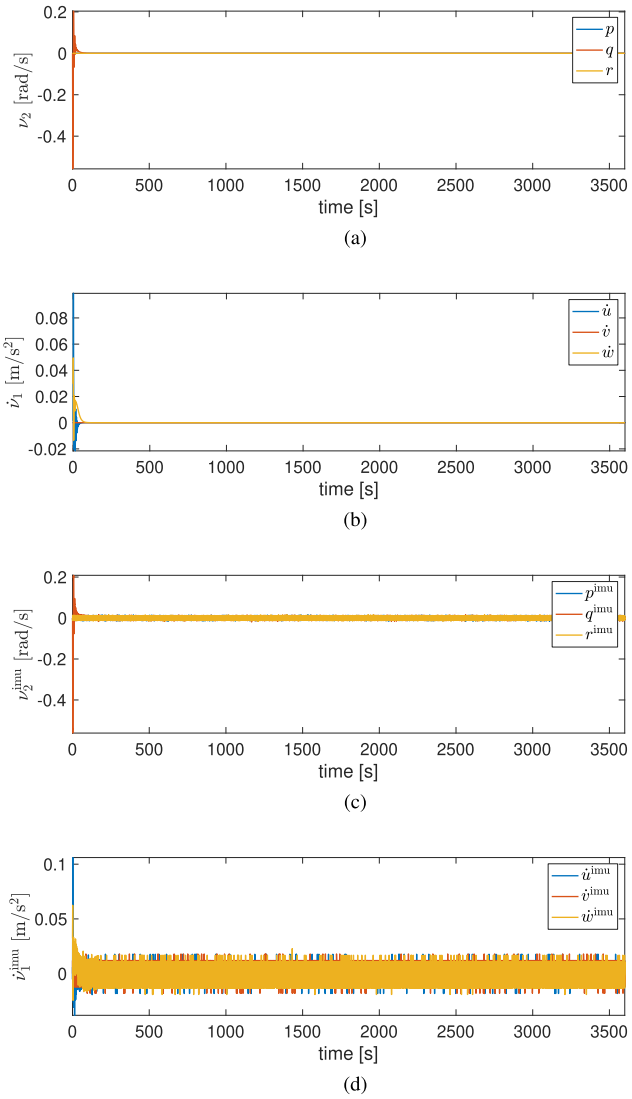

Fig. 6. True angular velocity and linear acceleration of a vehicle, and its noisy angular velocity and linear acceleration obtained from simulated IMU measurements. (a) True angular velocity. (b) True linear acceleration. (c) Noisy angular velocity from a simulated IMU. (d) Noisy linear acceleration from a simulated IMU.

TABLE IV

STATISTICAL PROPERTIES OF ANGULAR VELOCITY AND LINEAR ACCELERATION OBTAINED FROM THE SIMULATED IMU MEASUREMENTS SHOWN IN FIG. 6

Property	$\boldsymbol{\nu}_2^{\text{imu}}$	$\dot{\boldsymbol{\nu}}_1^{\text{imu}}$
Mean	$\begin{bmatrix} -0.0430 \\ 0.1213 \\ 0.0886 \end{bmatrix} \times 10^{-4}$	$\begin{bmatrix} 0.2984 \\ 0.4976 \\ 0.0229 \end{bmatrix} \times 10^{-5}$
Variance	$\begin{bmatrix} 0.1372 \\ 0.1369 \\ 0.1369 \end{bmatrix} \times 10^{-4}$	$\begin{bmatrix} 0.2025 \\ 0.2029 \\ 0.2032 \end{bmatrix} \times 10^{-4}$

the vehicle negative buoyant temporarily and the vehicle has IMU and depth sensors as its primary navigational sensors. Starting from $(x, y, z) = (0, 0, 0)$ (see the pentagram in Fig. 5) in the environment, the vehicle descends through the water column without active propulsion over the time interval of 1 h

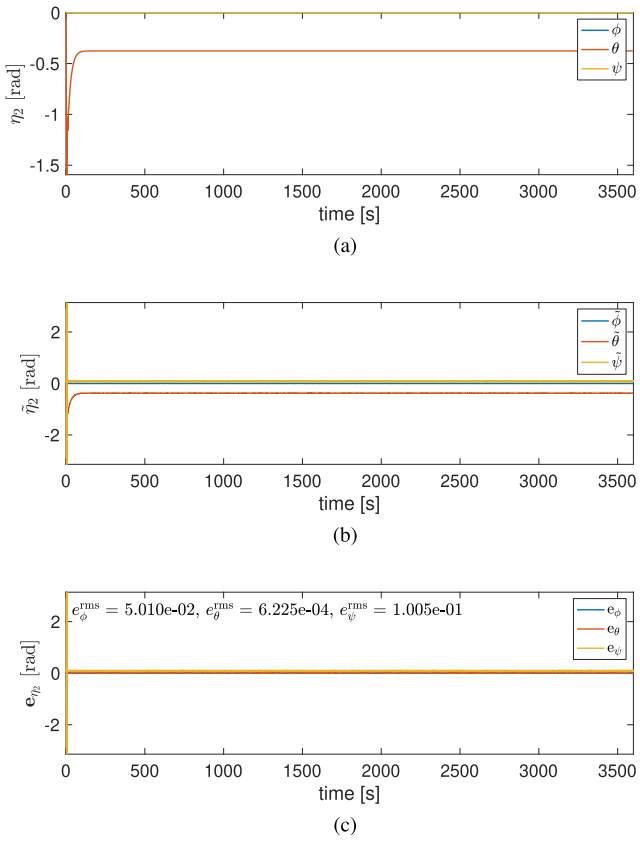

Fig. 7. Attitude estimation by the complementary filter provided by MATLAB using the noisy IMU data shown in Fig. 6 along with the magnetometer data (a) True orientation. (b) Estimated orientation. (c) Attitude estimation error.

Algorithm 2 Dead Reckoning

Input: Measurements from IMU and depth sensors
Output: Estimated vehicle state
1: $k = 0$.
2: Initialize the vehicle state $\boldsymbol{\chi}_k$.
3: **repeat**
4: $k = k + 1$.
5: Estimate orientation $\boldsymbol{\eta}_{2,k}^{\text{obs}}$ from an IMU.
6: Update position in $\boldsymbol{\chi}_k$ by integrating the processed $\dot{\boldsymbol{\nu}}_{1,k}^{\text{imu}}$.
7: **until** navigation is complete

to reach the sea bottom. In Sections VI-B and VI-C, using IMU and depth sensor measurements from the vehicle, we evaluate dead reckoning and nonactive perception (non-AP) as two baseline approaches followed by four implementations of the proposed framework for this case study of vehicle descent.

B. Vehicle Descent With Baseline Approaches

As the first baseline approach, we evaluate conventional dead reckoning (see Algorithm 2), for which we set $\boldsymbol{\tau}_k = \mathbf{0}$ for all k and keep the same IMU-related conditions applied to our approach, that is, dead reckoning is performed by using IMU measurements with time-varying bias and orientation estimated by complementary filter. Fig. 8 shows the dead-reckoning results. Even though dead reckoning incorporates

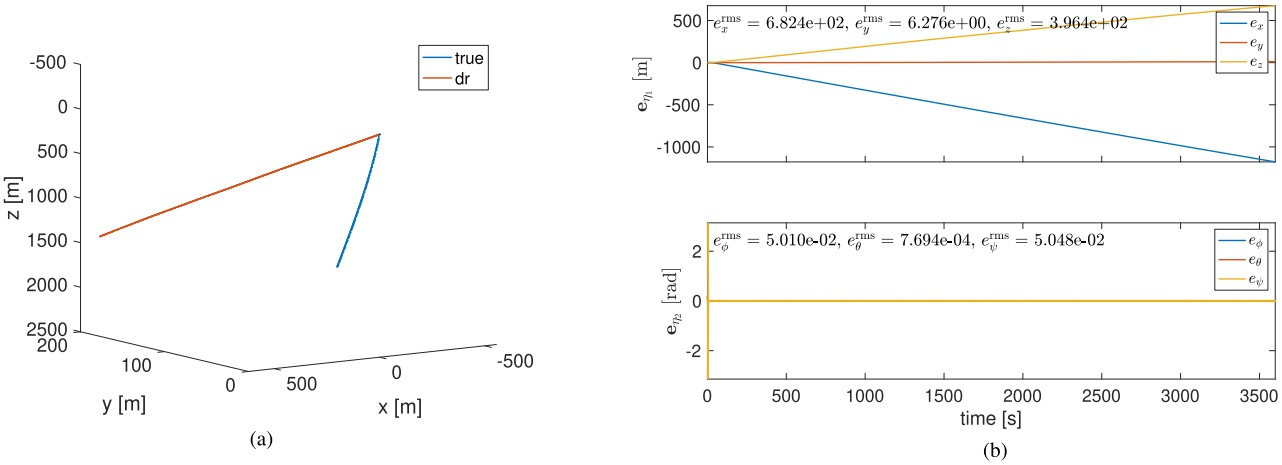

Fig. 8. Dead-reckoning results. (a) True (blue line) and dead-reckoned (red line) vehicle trajectories descending from $(x, y, z) = (0, 0, 0)$. (b) Dead-reckoning error. From the top, the position error $\mathbf{e}_{\eta_1}$ and orientation error $\mathbf{e}_{\eta_2}$ are provided. The rms errors in the individual axes are displayed in each plot.

TABLE V
ESTIMATION PERFORMANCE COMPARISON

	Dead-Reckoning	Non-AP	AP-OGwoDR	AP-CGwoDR	AP-OGwDR	AP-CGwDR
$\|\mathbf{e}_{\mathbf{f}_1}^{\text{rms}}\|$ $[m/s]$	N/A	1.16×10^{-2}	1.159×10^{-2}	1.016×10^{-3}	1.675×10^{-3}	1.984×10^{-3}
$\|\mathbf{e}_{\boldsymbol{\eta}_1}\|$ $[m]$	1357.950	35.695	35.522	1.8288	4.659	1.168
(% of dist traveled)	(69.445 %)	(1.668 %)	(1.657 %)	(0.085 %)	(0.218 %)	(0.054 %)

TABLE VI
SYSTEM NOISE PROPERTIES FOR STATE ESTIMATION

Property	Value	Property	Value
$\mathbf{Q}_k^{\chi_\mathrm{v}}$	$10^{-12} I_{12}$	$\mathbf{Q}_k^{\chi_{\mathbf{f}_1}}$	$10^{-10} I_3$
$\mathbf{R}_k^{\text{gyro}}$	$0.137 \times 10^{-4} I_3$	$\mathbf{R}_k^{\text{acc}}$	$0.2029 \times 10^{-4} I_3$
$\mathbf{R}_k^{\text{att}}$	$10^{-4} I_3$	R_k^{dr}	2×10^{-6}
R_k^{depth}	10^{-10}		

high-accuracy orientation estimates obtained from an attitude estimation algorithm, the position error grows over time since dead reckoning just integrates noisy IMU sensor measurements. Therefore, its performance is not desirable even for only 1-h descending. The localization error for dead reckoning is provided in Table V and compared with the results based on our proposed framework.

In addition to dead reckoning, we simulate vehicle state estimation without active perception control and flow state estimation as another baseline, referred to as non-AP, to compare with our proposed framework, that is, we implement Algorithm 1 while maintaining $\boldsymbol{\tau}_k = \mathbf{0}$ and $\mathbf{f}_{1,k} = \mathbf{f}_{1,0}$ for all k. System noise properties for state estimation are summarized in Table VI. For vehicle state estimation, we set the process noise $\boldsymbol{\xi}_k^{\chi_\mathrm{v}}$ in (19) to be zero-mean Gaussian with covariance $\mathbf{Q}_k^{\chi_\mathrm{v}} = 10^{-12} I_{12}$, that is, we assume that the vehicle dynamics are well represented by the vehicle motion model. The observation noise $\boldsymbol{\xi}_k^{\zeta_\mathrm{v}}$ in (25) to be zero-mean Gaussian with covariance $\mathbf{R}_k^{\zeta_\mathrm{v}} = \text{diag}(R_k^{\text{depth}}, \mathbf{R}_k^{\text{att}}, \mathbf{R}_k^{\text{gyro}}, \mathbf{R}_k^{\text{acc}})$ with $R_k^{\text{depth}} = 10^{-10}$, $\mathbf{R}_k^{\text{att}} = 10^{-4} I_3$, $\mathbf{R}_k^{\text{gyro}} = 0.137 \times 10^{-4} I_3$, and $\mathbf{R}_k^{\text{acc}} = 0.2029 \times 10^{-4} I_3$. Note that dead reckoning does not take the system noise into account while integrating the inertial sensor measurements.

Fig. 9 shows the results obtained by non-AP. Even though the estimation errors for the orientation and velocities of the vehicle are small [see rows 2–4 of Fig. 9(c)], as the growing error for the flow state [see Fig. 9(b)] is integrated in the estimation of the vehicle position, the estimation error for the vehicle position keeps increasing [see the first row of Fig. 9(c)], emphasizing the importance of flow state estimation. Note that the estimated position in the z-axis has a small error because it is directly estimated from the depth sensor measurement and the vertical flow is assumed to be zero. The norm of the root-mean-square (rms) errors for the flow state and the localization error along with the percentage of the distance traveled is shown in Table V.

C. Vehicle Descent With Active Perception

In this section, we present the simulation results generated through our proposed framework by using Algorithm 1. While a vehicle is descending, the proposed framework generates active perception control and estimates the vehicle and flow states using the IMU and depth sensor measurements. We use the same noise properties for vehicle state estimation used for non-AP in Section VI-B (see Table VI). For flow state estimation, the process noise $\boldsymbol{\xi}_k^{\chi_{\mathbf{f}_1}}$ in (26) is set to be zero-mean Gaussian with covariance $\mathbf{Q}_k^{\chi_{\mathbf{f}_1}} = 10^{-10} I_3$. Since the flow model (9) is derived under the assumption of time-invariant flow, we assume that the time-varying component of flow is driven by noise. Therefore, the covariance of the process noise for the flow state is set to account for the time-varying

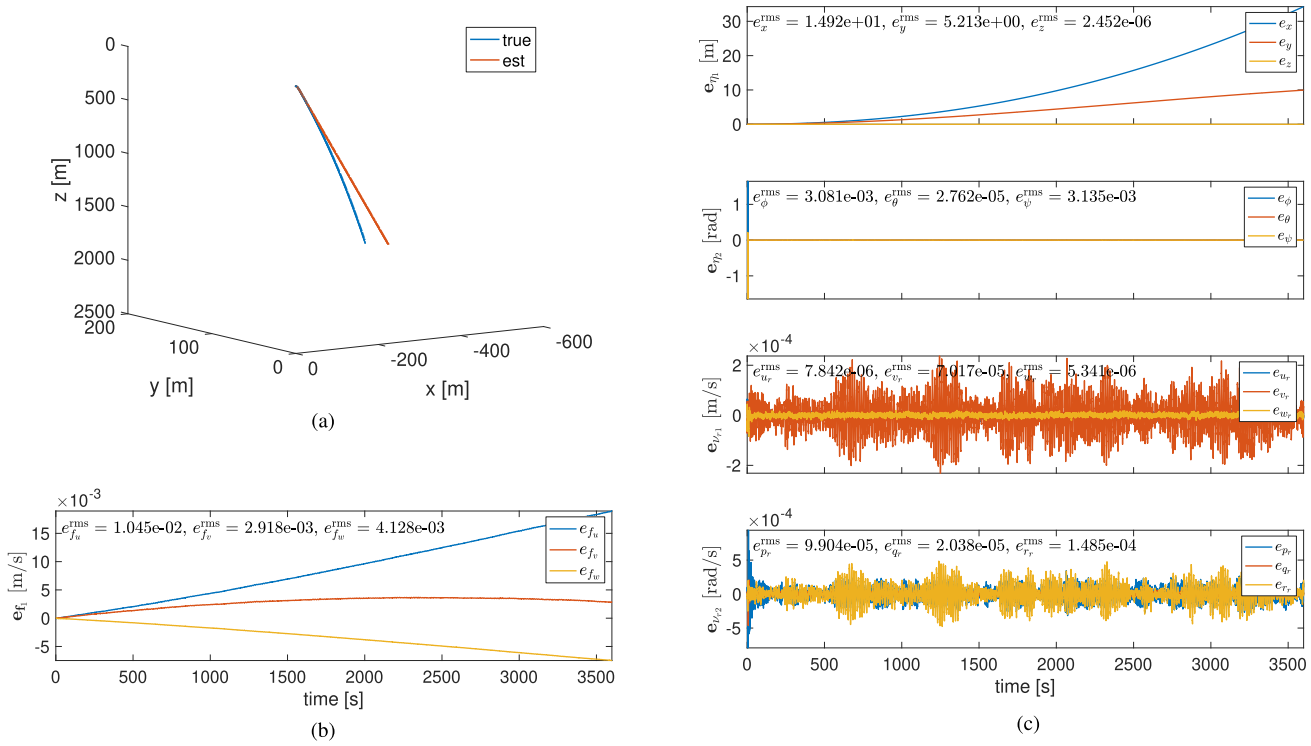

Fig. 9. Estimation results obtained through non-AP with the constant flow state (non-AP). (a) True (blue line) and estimated (red line) vehicle trajectories descending from $(x, y, z) = (0, 0, 0)$. (b) Error for the flow state, $\mathbf{e}_{\mathbf{f}_1}$. The rms errors in the individual axes are displayed in the plot. (c) Estimation error for the vehicle state. From the top, the position error $\mathbf{e}_{\boldsymbol{\eta}_1}$, orientation error $\mathbf{e}_{\boldsymbol{\eta}_2}$, linear velocity error $\mathbf{e}_{\boldsymbol{\nu}_{r1}}$, and angular velocity error $\mathbf{e}_{\boldsymbol{\nu}_{r2}}$ are provided. The rms errors in the individual axes are displayed in each plot.

dynamics of flow. The observation noise $\boldsymbol{\xi}_k^{\xi_{f_1}}$ in (29) is to be zero-mean Gaussian with covariance $\mathbf{R}_k^{\xi_{f_1}} = \text{diag}(\mathbf{R}_k^{\text{acc}}, \mathbf{R}_k^{\text{dr}})$ with $\mathbf{R}_k^{\text{acc}} = 0.2029 \times 10^{-4} I_3$ and $\mathbf{R}_k^{\text{dr}} = 2 \times 10^{-6}$.

To generate active perception control, we solve the following optimization problem:

$$\boldsymbol{\tau}_k^{\star} = \underset{\boldsymbol{\tau}_k}{\text{argmax}}\, \mathcal{F}_i^{\text{ap}} \tag{66}$$

$$\text{s.t. (11)}, \quad \text{(12)}, \tag{67}$$

$$|T_1|, \quad |T_2|, \quad |T_3|, \quad |T_4| \leq 0.1 \ N \tag{68}$$

where constraint (68) is added to keep control cost for active perception within a small bound. Please note that constraint (68) can be added to the cost function with an appropriate weighting constant using the Lagrangian relaxation [40] and the optimal solution may vary depending on the choice for the weighting constant. The optimization problem is solved by using the sequential quadratic programming in our simulations. Fig. 10 shows an example of control input generated by active perception.

To demonstrate the proposed framework, we simulate active perception with the following four conditions:

1) observability Gramian without the depth-rate measurement (AP-OGwoDR);
2) observability Gramian with the depth-rate measurement (AP-OGwDR);
3) constructability Gramian without the depth-rate measurement (AP-CGwoDR);

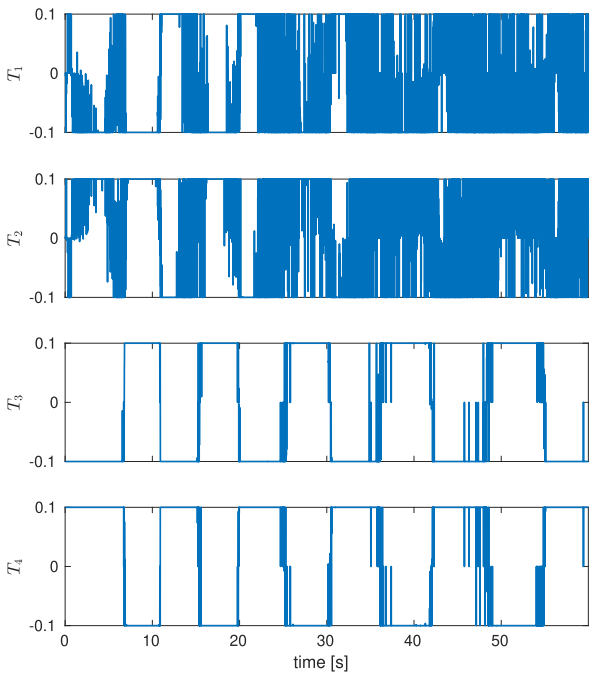

Fig. 10. Control input generated by active perception for the first 60 s of simulation. Thrusts vary to maximize $\lambda_{\min}$ of the Gramian.

4) constructability Gramian with the depth-rate measurement (AP-CGwDR).

As described in Section V-A, the observability Gramian and constructability Gramian are related in terms of uniform

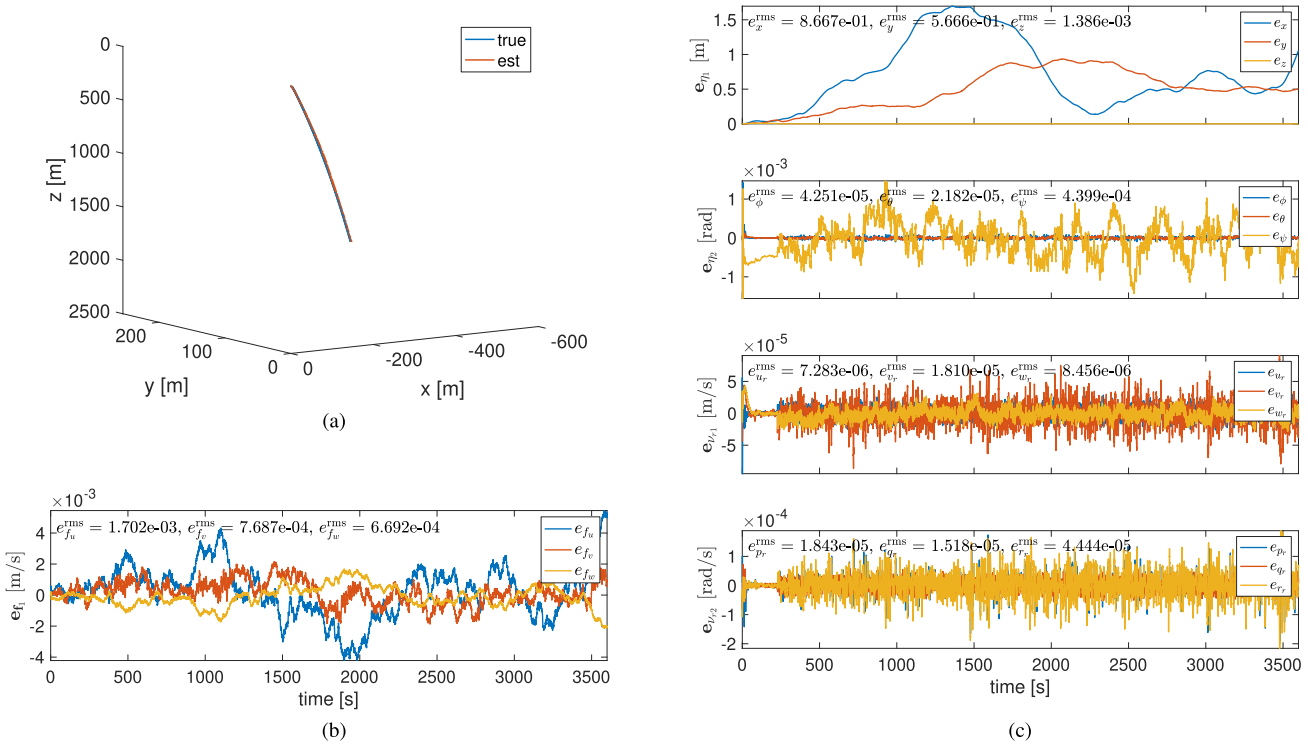

Fig. 11. Estimation results obtained through active perception using constructability Gramian with the depth-rate measurement (AP-CGwDR) (a) True (blue line) and estimated (red line) vehicle trajectories descending from $(x, y, z) = (0, 0, 0)$. (b) Estimation error for the flow state, $\mathbf{e}_{\mathbf{f}_1}$. The rms errors in the individual axes are displayed in the plot. (c) Estimation error for the vehicle state. From the top, the position error $\mathbf{e}_{\boldsymbol{\eta}_1}$, orientation error $\mathbf{e}_{\boldsymbol{\eta}_2}$, linear velocity error $\mathbf{e}_{\boldsymbol{\nu}_{r1}}$, and angular velocity error $\mathbf{e}_{\boldsymbol{\nu}_{r2}}$ are provided. The rms errors in the individual axes are displayed in each plot.

complete observability. We show how the proposed framework performs with additional past information incorporated in constructability Gramian compared to observability Gramian. In addition, a comparison of these conditions shows how our framework is affected by additional information of the depth-rate measurements. Table V shows the norm of the rms errors for the flow state and the localization error along with the percentage of the distance traveled.

AP-OGwoDR: Among four implementations of the proposed framework, the performance of AP-OGwoDR is noticeably worse. Note that we evaluate the observability Gramian for only one-step lookahead (i.e., $K = 1$). Without additional information of the depth-rate measurement, AP-OGwoDR does not have sufficient information to improve flow state estimation, resulting in localization performance in the same order as non-AP. This result improves significantly when the depth-rate measurement is incorporated into the proposed framework.

AP-XXwoDR Versus AP-XXwDR: Let us first compare AP-OGwoDR and AP-OGwDR. For observability Gramian with only one-step lookahead, additional information of the depth-rate measurement enables active perception control to improve flow state estimation, leading to enhanced vehicle state estimation and localization. However, comparing AP-CGwoDR and AP-CGwDR, since constructability Gramian takes past information into account along with one-step lookahead, incorporating the depth-rate measurement does not make much difference in flow and vehicle state estimation. To further analyze the effect of the depth-rate measurement in the proposed framework, we also compare control cost for the four active perception schemes (see Table VII). Although the estimation performance for AP-OGwDR, AP-CGwoDR, and AP-CGwDR is pretty close, with a combination of the depth-rate measurement and past information, AP-CGwDR has significant reduction in control cost for active perception.

TABLE VII
CONTROL COST COMPARISON

Thrust $[N]$	AP-OGwoDR	AP-CGwoDR	AP-OGwDR	AP-CGwDR
$\sum \lvert T_1 \rvert$	3.510×10^4	3.496×10^4	3.553×10^4	2.795×10^3
$\sum \lvert T_2 \rvert$	3.510×10^4	3.497×10^4	3.553×10^4	2.785×10^3
$\sum \lvert T_3 \rvert$	3.475×10^4	3.396×10^4	3.599×10^4	1.167×10^4
$\sum \lvert T_4 \rvert$	3.470×10^4	3.405×10^4	3.599×10^4	1.168×10^4
Total	1.397×10^5	1.379×10^5	1.430×10^5	2.893×10^4

Overall: As shown in Table V, since AP-OGwDR, AP-CGwoDR, and AP-CGwDR have similar estimation performance, we only provide the results obtained by AP-CGwDR shown in Fig. 11. Of these three, AP-CGwDR is the most auspicious considering its low estimation error and low control cost. The overall results show that the proposed framework can improve flow state estimation using active perception control and further achieve the enhanced vehicle state estimation even using IMU data with time-varying bias.

Note that the presented results are based on the optimization problem designed in (66)–(68). Disparate conditions in constraints may change the results. Finally, although the framework is validated for a specific case study, it can be extended as long as vehicle motion can be designed to improve flow state observability.

VII. Conclusion and Future Work

This article has proposed an active perception framework for AUV navigation using IMU and depth sensors only. The proposed framework is established by employing vehicle and flow motion models that incorporate the coupling between vehicle motion and ocean flow. With these models, a nonlinear system for the vehicle state and a linear time-varying system for the flow state are separately constructed, facilitating flow state estimation. Due to coupling, observability for the flow state depends on vehicle motion. To achieve the observability for the flow state, active perception control exploits vehicle motion and maximizes an information metric pertaining to estimation performance based on either observability or constructability Gramian for the flow state. While a vehicle is in motion with active perception control, the vehicle and flow states are estimated by separate filters, in which the estimated states are jointly used for estimation of the other state. The simulation results demonstrate the effectiveness of the proposed framework for AUV navigation.

The proposed framework relies on a model-based analysis, but in real deployments, model uncertainty may significantly impact its performance. Therefore, we will conduct a robustness analysis for the framework to address practical applicability. In addition, for field trials, it is also important to consider sampling and control frequencies to make the framework real-time feasible. In extending the framework to various navigation tasks, we will investigate a more general formulation of active perception control instead of considering it as input injection. Finally, we plan to incorporate bias estimation and also analyze theoretical or empirical bounds on the estimated variables.

Acknowledgment

The authors would like to thank Niankai Yang at the University of Michigan, Ann Arbor, MI, USA, for helpful discussion during the course of the study.

References

[1] F. Zhang, G. Marani, R. N. Smith, and H. T. Choi, "Future trends in marine robotics [TC spotlight]," *IEEE Robot. Autom. Mag.*, vol. 22, no. 1, pp. 114–122, Mar. 2015.

[2] J. C. Kinsey, R. Eustice, and L. L. Whitcomb, "A survey of underwater vehicle navigation: Recent advances and new challenges," in *Proc. IFAC Conf. Manoeuvring Control Mar. Craft*, 2006, pp. 1–12.

[3] P. A. Miller, J. A. Farrell, Y. Zhao, and V. Djapic, "Autonomous underwater vehicle navigation," *IEEE J. Ocean. Eng.*, vol. 35, no. 3, pp. 663–678, Jul. 2010.

[4] L. Paull, S. Saeedi, M. Seto, and H. Li, "AUV navigation and localization: A review," *IEEE J. Ocean. Eng.*, vol. 39, no. 1, pp. 131–149, Jan. 2014.

[5] D. Chang, F. Zhang, and C. R. Edwards, "Real-time guidance of underwater gliders assisted by predictive ocean models," *J. Atmos. Ocean. Technol.*, vol. 32, no. 3, pp. 562–578, 2015.

[6] T. O. Fossum *et al.*, "Information-driven robotic sampling in the coastal ocean," *J. Field Robot.*, vol. 35, no. 7, pp. 1101–1121, Oct. 2018.

[7] K. Ma, L. Liu, H. K. Heidarsson, and G. S. Sukhatme, "Data-driven learning and planning for environmental sampling," *J. Field Robot.*, vol. 35, no. 5, pp. 643–661, Aug. 2018.

[8] J. Osborn, S. Qualls, J. Canning, M. Anderson, D. Edwards, and E. Wolbrecht, "AUV state estimation and navigation to compensate for ocean currents," in *Proc. OCEANS MTS/IEEE Washington*, Oct. 2015, pp. 1–5.

[9] E. Wolbrecht *et al.*, "Estimating and compensating for water currents: Field testing," in *Proc. OCEANS MTS/IEEE Monterey*, Sep. 2016, pp. 1–5.

[10] I. Klein and R. Diamant, "Observability analysis of DVL/PS aided INS for a maneuvering AUV," *Sensors*, vol. 15, no. 10, pp. 26818–26837, 2015.

[11] L. Medagoda, S. B. Williams, O. Pizarro, J. C. Kinsey, and M. V. Jakuba, "Mid-water current aided localization for autonomous underwater vehicles," *Auton. Robots*, vol. 40, no. 7, pp. 1207–1227, Oct. 2016.

[12] Z. Song and K. Mohseni, "Long-term inertial navigation aided by dynamics of flow field features," *IEEE J. Ocean. Eng.*, vol. 43, no. 4, pp. 940–954, Oct. 2018.

[13] E. Kim, S. Fan, and N. Bose, "Estimating water current velocities by using a model-based high-gain observer for an autonomous underwater vehicle," *IEEE Access*, vol. 6, pp. 70259–70271, 2018.

[14] Z. Song and K. Mohseni, "Concurrent flow-based localization and mapping in time-invariant flow fields," in *Proc. IEEE/RSJ Int. Conf. Intell. Robots Syst. (IROS)*, Nov. 2019, pp. 7205–7210.

[15] D. Chang, M. Johnson-Roberson, and J. Sun, "An active perception approach for mid-water localization of autonomous underwater vehicles," in *Proc. Amer. Control Conf. (ACC)*, Jul. 2020, pp. 671–676.

[16] N. Crasta, M. Bayat, A. P. Aguiar, and A. M. Pascoal, "Observability analysis of 3D AUV trimming trajectories in the presence of ocean currents using range and depth measurements," *Annu. Rev. Control*, vol. 40, pp. 142–156, 2015.

[17] S. Zhang, J. Yu, A. Zhang, and F. Zhang, "Spiraling motion of underwater gliders: Modeling, analysis, and experimental results," *Ocean Eng.*, vol. 60, pp. 1–13, Mar. 2013.

[18] F. Zhang, F. Zhang, and X. Tan, "Tail-enabled spiraling maneuver for gliding robotic fish," *J. Dyn. Syst., Meas., Control*, vol. 136, no. 4, pp. 1–8, Jul. 2014.

[19] R. Bajcsy, Y. Aloimonos, and J. Tsotsos, "Revisiting active perception," *Auto. Robots*, vol. 42, pp. 177–196, May 2018.

[20] A. Arora, P. M. Furlong, R. Fitch, S. Sukkarieh, and T. Fong, "Multi-modal active perception for information gathering in science missions," *Auto. Robots*, vol. 43, no. 7, pp. 1827–1853, Oct. 2019.

[21] G. A. Hollinger and G. S. Sukhatme, "Sampling-based robotic information gathering algorithms," *Int. J. Robot. Res.*, vol. 33, no. 9, pp. 1271–1287, Aug. 2014.

[22] A. Kim and R. M. Eustice, "Active visual SLAM for robotic area coverage: Theory and experiment," *Int. J. Robot. Res.*, vol. 34, nos. 4–5, pp. 457–475, 2015.

[23] A. Munafo, G. Ferri, K. LePage, and R. Goldhahn, "AUV active perception: Exploiting the water column," in *Proc. OCEANS Aberdeen*, Jun. 2017, pp. 1–8.

[24] K. M. B. Lee, J. J. H. Lee, C. Yoo, B. Hollings, and R. Fitch, "Active perception for plume source localisation with underwater gliders," in *Proc. Australas. Conf. Robot. Autom.*, 2018, pp. 1–10.

[25] T. I. Fossen, *Handbook of Marine Craft Hydrodynamics and Motion Control*. Hoboken, NJ, USA: Wiley, 2011.

[26] G. Antonelli, *Underwater Robots* (Springer Tracts in Advanced Robotics), vol. 96. Cham, Switzerland: Springer, 2014, doi: 10.1007/978-3-319-02877-4.

[27] R. Hermann and A. J. Krener, "Nonlinear controllability and observability," *IEEE Trans. Autom. Control*, vol. AC-22, no. 5, pp. 728–740, Oct. 1977.

[28] A. J. Krener and K. Ide, "Measures of unobservability," in *Proc. 48th IEEE Conf. Decis. Control (CDC) Jointly 28th Chin. Control Conf.*, Dec. 2009, pp. 6401–6406.

[29] B. Allotta, R. Costanzi, F. Fanelli, N. Monni, L. Paolucci, and A. Ridolfi, "Sea currents estimation during AUV navigation using unscented Kalman filter," *IFAC-PapersOnLine*, vol. 50, no. 1, pp. 13668–13673, 2017.

[30] R. E. Kalman and R. S. Bucy, "New results in linear filtering and prediction theory," *J. Basic Eng.*, vol. 83, no. 1, pp. 95–108, 1961.

[31] A. H. Jazwinski, *Stochastic Processes and Filtering Theory*. New York, NY, USA: Dover, 1970.

[32] W. Li and J. Wang, "Magnetic sensors for navigation applications: An overview," *J. Navigat.*, vol. 67, no. 2, pp. 263–275, Mar. 2014.
[33] D. Gebre-Egziabher, R. C. Hayward, and J. D. Powell, "A low-cost GPS/inertial attitude heading reference system (AHRS) for general aviation applications," in *Proc. IEEE Position Location Navigat. Symp.*, Apr. 1998, pp. 518–525.
[34] R. Mahony, T. Hamel, and J.-M. Pflimlin, "Nonlinear complementary filters on the special orthogonal group," *IEEE Trans. Autom. Control*, vol. 53, no. 5, pp. 1203–1218, Jun. 2008.
[35] R. G. Valenti, I. Dryanovski, and J. Xiao, "Keeping a good attitude: A quaternion-based orientation filter for IMUs and MARGs," *Sensors*, vol. 15, no. 8, pp. 19302–19330, 2015.
[36] J. Kiefer and J. Wolfowitz, "Optimum designs in regression problems," *Ann. Math. Statist.*, vol. 30, pp. 271–294, Jun. 1959.
[37] P. C. Müller and H. I. Weber, "Analysis and optimization of certain qualities of controllability and observability for linear dynamical systems," *Automatica*, vol. 8, no. 3, pp. 237–246, May 1972.
[38] P. Salaris, M. Cognetti, R. Spica, and P. R. Giordano, "Online optimal perception-aware trajectory generation," *IEEE Trans. Robot.*, vol. 35, no. 6, pp. 1307–1322, Dec. 2019.
[39] S. C. Shadden, F. Lekien, and J. E. Marsden, "Definition and properties of Lagrangian coherent structures from finite-time Lyapunov exponents in two-dimensional aperiodic flows," *Phys. D, Nonlinear Phenomena*, vol. 212, nos. 3–4, pp. 271–304, Dec. 2005.
[40] M. L. Fisher, "The Lagrangian relaxation method for solving integer programming problems," *Manage. Sci.*, vol. 27, no. 1, pp. 1–18, Jan. 1981.

Dongsik Chang (Member, IEEE) received the B.S. degree in electrical and computer engineering from Hanyang University, Seoul, South Korea, in 2007, and the M.S. and Ph.D. degrees in electrical and computer engineering the Georgia Institute of Technology, Atlanta, GA, USA, in 2010 and 2016, respectively.

After the completion of his Ph.D. degree, he spent about two years in industry, working with Samsung Electronics, Seoul, as a Senior Engineer. He is currently a Postdoctoral Scholar with Oregon State University, Corvallis, OR, USA. Before joining Oregon State University, he held a Research Fellow position at the University of Michigan, Ann Arbor, MI, USA. His research lies at the intersection of systems and control, and robotics. His research interests include marine robotics, active perception, intelligent autonomous systems, control theory, mobile sensor networks, multiagent systems, and machine learning.

Matthew Johnson-Roberson received the Ph.D. degree from The University of Sydney, Camperdown, NSW, Australia, in 2010.

He is currently an Associate Professor of Engineering with the Department of Naval Architecture and Marine Engineering and the Department of Electrical Engineering and Computer Science, University of Michigan, Ann Arbor, MI, USA, where he co-directs the UM Ford Center for Autonomous Vehicles, and he founded and leads the Deep Robot Optical Perception Laboratory, which researches 3-D reconstruction, segmentation, data mining, and visualization. He has held prior post-doctoral appointments at the Centre for Autonomous Systems, KTH Royal Institute of Technology, Stockholm, Sweden, and the Australian Centre for Field Robotics, The University of Sydney.

Dr. Johnson-Roberson was a recipient of the NSF CAREER Award in 2015.

Jing Sun (Fellow, IEEE) received the Ph.D. degree from the University of Southern California, Los Angeles, CA, USA, in 1989.

She is currently the Michael G. Parsons Collegiate Professor with the Department of Naval Architecture and Marine Engineering, with joint appointments at the Department of Electrical Engineering and Computer Science, and the Department of Mechanical Engineering, University of Michigan, Ann Arbor, MI, USA. Her research interests include modeling, control, and optimization of dynamic systems, with applications to marine and automotive systems.

Dr. Sun is a fellow of the National Academy of Inventors, the International Federation of Automatic Control (IFAC), and the Society of Naval Architects and Marine Engineers. She was a recipient of the 2003 IEEE Control System Technology Award.